# New insights into how MutS separates its function in the regulation of the Pol IV access to replication sites from that in the conserved MMR pathway

Milagros Inés Ibáñez Busseti[1], Lucía Malvina Margara[1], Sofía Daiana Castell[1], Marisa Mariel Fernández[2], Emilio Luis Malchiodi[2], Guillermo Gabriel Montich[1], Virginia Miguel[3], Carlos Enrique Argaraña[1] and Mariela Roxana Monti[1,*]

[1]Centro de Investigaciones en Química Biológica de Córdoba (CIQUIBIC), CONICET, Departamento de Química Biológica Ranwell Caputto, Facultad de Ciencias Químicas, Universidad Nacional de Córdoba, Ciudad Universitaria, Córdoba, X5000HUA, Argentina.

[2]Cátedra de Inmunología and Instituto de Estudios de la Inmunidad Humoral Profesor Ricardo A. Margni, CONICET, Facultad de Farmacia y Bioquímica, Universidad de Buenos Aires, Buenos Aires, C1113AAD, Argentina.

[3]Instituto de Investigaciones Biológicas y Tecnológica, CONICET, Facultad de Ciencias Exactas, Físicas y Naturales, Universidad Nacional de Córdoba, Córdoba, Argentina.

* To whom correspondence should be addressed. Tel: 54-351-5353855; E-mail: mariela.monti@unc.edu.ar

**ABSTRACT**

MutS removes mutagenic replication errors by initiating the mismatch repair (MMR) or the regulation of specialized DNA polymerases (RSP) pathways. This factor recognizes mismatches in double-stranded DNAs, and following ADP-ATP exchange, forms a sliding clamp that recruits MutL during MMR. In the RSP pathway, mismatch-bound MutS controls interaction of the low-fidelity Pol IV with the processivity factor assembled onto primed DNA (pDNA) sites. Here, we demonstrated that MutS associates with pDNAs by binding to a novel DNA interaction surface, in which Arg 272 appeared to directly interact with the 3'-end. Mutation of this conserved Arg conferred a noticeable defect in mismatch binding and the MutS antimutagenic activity *in vivo*. MutS interaction with mismatched pDNAs inhibited ADP-ATP exchange and transition into a sliding clamp, and decreased MutS affinity for MutL. Hence, replication DNA structures modulate pathway choice, which is critical to ensure the maintenance of genome stability.

**KEYWORDS**

MutS; MutL; mismatch repair; DNA replication; specialized DNA polymerases; mutagenesis; Pseudomonas aeruginosa

## INTRODUCTION

Most living organisms possess the DNA mismatch repair (MMR) mechanism in order to avoid mutations and safeguard genomic stability. MMR corrects mismatches and insertion-deletion loops generated during DNA synthesis, enhancing the overall fidelity of DNA replication up to 1000-fold (1). MMR also plays critical roles in other cellular biological processes such as mitotic and meiotic recombination, and DNA-damage signaling. Defects in MMR factors are associated with a mutator phenotype, characterized by increased mutation and recombination rates, and result in an increased susceptibility to sporadic colorectal, endometrial and ovarian cancer in humans (2).

Repair reactions leading to the correction of replication errors have been studied over the last 30 years, using *in vitro* structural analysis and bulk and single-molecule biochemical experiments (1,3). The essential MMR steps comprise error recognition, discrimination of the nascent strand containing the error, strand excision and gap-filling DNA synthesis. These reactions are catalyzed by the core MMR machinery, including the highly conserved MutS and MutL proteins (and eukaryotic MutSα, MutSβ and MutLα), and accessory factors involved in other DNA metabolic pathways.

MMR is initiated by the mismatch sensing MutS protein, which belongs to the ATP-binding cassette ATPase family (4,5). ADP-bound MutS moves along the double-stranded DNA, searching for mismatches. Error recognition stalls the diffusion of MutS at the site of the mismatch and triggers the exchange of ADP by ATP (6-9). ATP binding elicits a MutS conformational transition into a sliding clamp that dissociates from the mismatch in an ATP hydrolysis-independent manner and recruits MutL (6,9-11). This ATP-bound MutS sliding clamp is critical for MMR as it communicates mismatch recognition to downstream MMR components involved in the strand discrimination and excision steps. These MMR reactions are different between a subset of enteric bacteria, including *Escherichia coli*, and all other bacteria and eukaryotes. In *E. coli*, MutL activates the MutH endonuclease, which incises the unmethylated nascent strand in hemi-methylated d(GATC) sites (6,11). This transient hemi-methylated status provides a strand discrimination signal during the MutH nicking reaction as DNA adenine methylase (Dam) modifies d(GATC) sequences shortly after replication (12). The UvrD helicase unwinds the DNA starting from the nick, followed by strand degradation by single-stranded DNA exonucleases (13-15). The mechanism of strand-specific incision and excision remains poorly understood in bacteria and eukaryotes lacking Dam and MutH. In these organisms, MutL contains a latent endonuclease activity that introduces incisions used as an entry site for excision factors (16). This nicking activity is stimulated by interaction with MutS and/or replication processivity factors, the prokaryotic β clamp and the archaeal/eukaryotic proliferating cell nuclear antigen (PCNA) (15,17-21). Association with asymmetrically-loaded processivity factors also plays a role in directing the MutL incision to the nicked (nascent) strand (17-19). Moreover, transient nicks associated with DNA synthesis or introduced during removal of misincorporated ribonucleotides from DNA could be used as starting points of excision and thus, also act as strand discrimination signals (22-24). In the final repair steps, a DNA polymerase resynthesizes the resulting excision gap and a DNA ligase seals any remaining strand nicks.

It has been recently described a noncanonical function of MutS in the regulation of specialized DNA polymerases (RSP) that also contributes to maintain replication fidelity. Specialized DNA polymerases (Pol) relieve stalled replication forks, by assisting high-fidelity replicative Pols during synthesis across DNA damaged templates, but also display a potentially deleterious mutagenic activity (25). In *Pseudomonas aeruginosa*, MutS modulates access of the low-fidelity Pol IV to replication sites by controlling its association with β clamp (26). This ring-shaped factor targets Pol IV to DNA synthesis sites through binding of the conserved binding motif (CBM) of Pol IV to one of the two hydrophobic clefts on the surface of the ring (27). This novel pathway is initiated by the recruitment of Pol IV to stalled replication machineries. Subsequently, the specialized Pol gains access to the primer terminus from the replicative Pol III holoenzyme (conformed by Pol III α and ε, β clamp ,and the DnaX clamp loader) by binding to one cleft of β clamp while Pol III remains bound to the second cleft. If Pol IV incorporates an incorrect nucleotide, MutS is recruited as its affinity for β clamp increases in the presence of mispairs located close to a primed site. Then, the repair protein competes Pol IV off β clamp by interacting with the cleft occupied by Pol IV, which results

in the excision of the incorrect nucleotide by the exonuclease activity of Pol III. After error removal, MutS leaves the processivity factor and Pol III resumes the processive DNA synthesis. Although this pathway works in the context of stalled replisomes, it could also function to remove incorrect nucleotides inserted by Pol IV during bypass reactions in lesion-containing gaps left behind replisomes. The mechanism used by MutS to control specialized Pols differs in eukaryotes. Human MutSα facilitates recruitment of Pol κ and Pol η and their exchange with replicative Pols for accurate lesion bypass by promoting monoubiquitination of PCNA (28,29).

Control of specialized Pols by MutS is predicted to occur at replication sites as this novel role of the repair factor depends on its direct or functional interaction with processivity factors (30,31). Remarkably, MutS must eventually contact β clamp molecules resident in replisomes as the Pol III-Pol IV switch takes place at replication forks (26). In addition, substantial evidence demonstrates a spatiotemporal coupling of the mismatch repair process with DNA replication, which is thought to facilitate recognition of mismatches and encountering DNA replication-associated signals used during strand discrimination (3,32). MMR activity is highest during S-phase in eukaryotic cells (33). The core MMR proteins, MutS and MutL, have been found to directly bind to components of the DNA replication machinery (34-40). Notably, MutS tracks with the replisome and persists transiently behind the advancing replication forks in living cells (41,42). This localization has been ascribed to interactions between MutS and replication proteins, but it is independent of the number of DNA mismatches or the ability of MutS to recognize them (40-45). MutL forms foci dependent on MutS that rarely colocalize with MutS or replication factors (40,43,46,47). In the context of the MMR pathway, it has been suggested that MutS transiently moves with the replication apparatus until a mismatch is recognized, which induces uncoupling of MutS from the replication fork to initiate the recruitment of MutL. MutS could load several MutL molecules onto DNA at or close to the mismatch site, resulting in the formation of active sites of repair (32).

An important question to resolve is how MutS separates its function in the regulation of specialized Pols from that in the conserved DNA mismatch repair pathway. It seems a challenging task in view of the fact that both pathways are initiated by MutS mismatch recognition and take place at DNA replication sites. Findings obtained in the present work reveal factors influencing pathway choice for the reversion of replication errors.

## MATERIALS AND METHODS

Methods for construction of plasmids for protein expression, purification of recombinant proteins and preparation of DNA substrates are detailed in Supplementary Data.

### Native polyacrylamide gel electrophoresis

Native polyacrylamide gel electrophoresis assays were carried out by incubating affinity-purified proteins in the presence or absense of DNA oligonucleotides in binding buffer (20 mM Tris-HCl, pH 7.4, 5 mM $MgCl_2$, 1 mM dithiothreitol, 25 mM NaCl and 100 µg/ml BSA) for 25 min at 30°C. Samples were applied to native polyacrylamide gels prepared in Tris-borate buffer and run at 4°C. The gels were stained with ethidium bromide and coomassie blue, and the intensity of protein or DNA bands was quantified using the Gel-Pro analyzer software (MediaCybernetics, Silver Spring, MD, USA). Additional details are described in Supplementary Data.

### Surface plasmon resonance

Surface plasmon resonance analysis was performed using a BIAcore T100 instrument (GE Healthcare) at 25°C. Biotinylated DNA substrates and proteins were immobilized on a streptavidin-derivatized sensor chip or a CM5 chip surface by amine coupling, respectively. Soluble proteins were diluted in the 20 mM Tris-HCl, pH 7.4, 10 mM $MgCl_2$, 1 mM dithiothreitol and 25 mM NaCl, and injected over chip surfaces at a flow rate of 30 µl $min^{-1}$. Additional details are described in the Supplementary Data.

### Dot far-western blotting

These assays were performed as previously described (36) with minor modifications as detailed in the Supplementary Data.

### Circular dichroism

Far-UV CD spectra of 2 µM MutS preincubated alone or with DNA substrates (4 µM) in 6 mM Tris-HCl, pH 7.4, 7.5 mM NaCl and 0.28% glycerol were recorded using a Chirascan CD spectroscope (Applied Photophysics). Spectra were collected in triplicate from 250 nm to 190 nm at 25°C. The prediction of the proportion of the secondary structural element contents was performed using the BeStSel server available on the Web (http://bestsel.elte.hu/) (48).

### Limited proteolysis

2 µM MutS was preincubated alone or with DNA substrates (4 µM) in binding buffer for 1 h at 4°C. Then, mixtures were reacted with trypsin (7.3-13 µg/ml) for 10 min at 37 °C. Proteolysis reactions were quenched by the addition of sample buffer and boiled for 10 min. The proteolytic products were separated on 8% SDS-polyacrylamide gel and Coomassie blue stained. The full length-MutS band intensity was quantified using the Gel-Pro analyzer.

### ATPase activity

To measure the ATPase activity of MutS, MutSR272E and MutSF33A proteins (20-1280 nM) were mixed with 200 µM ATP in binding buffer. To determine the effect of DNAs on the ATP hydrolysis catalyzed by MutS, reaction mixtures contained 40 nM MutS, 1.6 µM DNA and ATP (3-400 µM) in binding buffer. Reactions were initiated by the addition of MutS and incubated for 20 min at 37°C. The liberation of phosphate from ATP was determined by using the malachite green assay. Briefly, the malachite green dye mixture (0.09% malachite green dye, 1.48% ammonium molybdate and 0.17% Tween 20) was added in a 1:4 ratio to reactions and incubated for 15 min at room temperature prior to being read at 612 nm. The standard curve was measured using $NaH_2PO4$ solution.

### Endonuclease activity

DNA substrates (1 µM) were incubated with MutL (0.13-1.3 µM) alone or in the presence of MutS or β clamp (0.13 µM) in the endonuclease buffer (20 mM Tris-HCl, pH 7.4, 30 mM NaCl, 5

mM $MnCl_2$ and 5 mM $MgCl_2$). Following a 2-h incubation at 37°C, reactions were stopped by adding 25 mM EDTA and 1 mg/ml proteinase K, and incubated for 30 min at 55°C. Reaction mixtures were resolved on 16 % native polyacrylamide gels prepared in Tris-borate buffer and run at 4°C. DNA was visualized by ethidium bromide staining. Quantification of DNA was done using the Gel-Pro program.

**Prediction of putative DNA binding residues**

MutS putative DNA binding sites were evaluated using the DNA binding predictor BindUp (http://bindup.technion.ac.il/) (49). For molecular docking, rigid 3D structural models of the DNA substrates were generated using **Make-na** (http://structure.usc.edu/make-na/) (50) and **3D-DART** (51). Molecular docking between the MutS crystal structure (PDB: 1E3M) and DNA substrates was performed using **HDOCK** server (52). MutS-DNA figure renders were obtained using VMD (53).

**Estimation of spontaneous mutation rates**

Mutation rates of *P. aeruginosa* PAO1 *mutS* containing pEx vectors were determined by the modified Luria-Delbruck fluctuation test as detailed in the Supplementary Data.

## RESULTS

### Replication DNA substrates are recognized by MutS

Biochemical studies have proved the extraordinary capacity of MutS proteins to recognize a broad range of DNA substrates. The repair factor can bind to mispairs and deletion/insertion loops as well as damaged bases present in MMR double-stranded DNA substrates (dsDNA). MutS is also able to associate with other DNA structures like D-loops, four-stranded Holliday junctions and G quadruplexes (54-56). However, and to our knowledge, no studies have evaluated MutS interaction with replication primed DNA structures (pDNA). With this aim, MutS from *P. aeruginosa* (hereinafter referred to as MutS) was purified and its ability to bind to replication DNA substrates was tested by surface plasmon resonance (29) and electrophoretic mobility shift assays (EMSA). These substrates included a matched pDNA, conformed by a 27-nt primer strand and a 37-nt template strand, and a GT mismatched pDNA (GT-pDNA), which contained a GT mismatch 8 nt from the 3'-hydroxyl (OH) terminus (Figure 1A). A dsDNA (37nt/37nt) and a GT-dsDNA, containing the mismatch centrally located, were used as controls.

The SPR measurements showed that MutS specifically bound to GT-pDNA (Figure 1B), exhibiting an apparent dissociation constant ($K_D$) of 230.0±0.9 nM as calculated by a nonlinear analysis considering the maximum response obtained for each concentration (Supplementary Figure S1A). DNA binding kinetics were analyzed by a global fit to a 1:1 Langmuir, a two-state reaction, and a two-state reaction with conformational changes mathematical models (Supplementary Figure S1B). The fit was poor, indicating that the MutS binding kinetic was not satisfied by these tested models. MutS also interacted with GT-dsDNA under the SPR conditions (Figure 1C). The kinetic data perfectly fitted to a global 1:1 Langmuir model, which allowed the calculation of the kinetic parameters, *k*on=(2.84±0.03) $10^3$ $M^{-1}$ $s^{-1}$ and *k*off=(28.8±0.6) $10^{-4}$ $s^{-1}$, and the kinetic $K_D$=1014 nM. It was not possible to estimate $K_D$ from analysis of equilibrium binding data as maximum response units did not reach a plateau at the highest MutS concentrations tested.

MutS was able to bind to all DNA substrates in EMSA assays (Supplementary Figure S1C to S1F). The plot of the DNA bound fraction as a function of free MutS concentrations fitted to a sigmoidal curve for all DNAs, indicating a cooperative interaction independently of the type of DNA structure. MutS displayed a strong interaction with GT-pDNA ($K_D$= 334±38 nM) while its binding affinity was slightly weaker for pDNA ($K_D$= 448±15 nM). As expected, MutS exhibited a high affinity for GT-dsDNA ($K_D$= 374±29 nM) whereas it bound to dsDNA with low efficiency ($K_D$= 2901±26 nM). Taken together, our findings clearly indicate that MutS specifically binds to replication DNA structures, exhibiting similar binding affinities for GT-pDNA and pDNA as GT-dsDNA.

### Replication DNA substrates containing a mismatch alters MutS electrophoretic migration under native conditions

We next analyzed the mobility of the MutS-DNA complexes on native gels, which could provide information on their size or conformation. MutS was incubated in the absence or presence of DNA substrates and then, subjected to electrophoretic analysis. Gels were stained with ethidium bromide and subsequently with coomassie blue to detect DNA and protein, respectively, in all assays. We identified MutS-DNA complexes as bands that showed both ethidium bromide and coomassie blue staining (Supplementary Figure S2A). Coomassie-stained gels are shown from now on for simplicity. In the absence of DNA, MutS migrated as a single band corresponding to a molecular weight of ~448 kDa (band b, Figure 1D), indicating that the protein is mainly a tetramer since the estimated molecular mass of the MutS monomer is 95 kDa. MutS bound to GT-pDNA exhibited a significant shift in mobility (band a, Figure 1D). ~90% of the protein migrated as a band near ~331 kDa, which could be due to a change in the oligomeric state from tetramer to dimer or a conformational rearrangement to a more compact protein structure. Conversely, MutS complexed with GT-dsDNA showed a decreased mobility as ~92% of the protein-DNA complex migrated at ~694 kDa (band c, Figure 1D). dsDNA (~631 kDa) and pDNA (~685 kDa) induced a similar effect on MutS migration to that observed for GT-dsDNA (Figure 1D). This decreased migration could be due to a more extended conformation adopted by the MutS tetramer upon binding to these DNA substrates or binding of multiple tetramers on a single DNA molecule.

In order to gain insight into the structural DNA features responsible for inducing a faster mobility of MutS by GT-pDNA, we determined the effect of extending the 3'-OH terminus of the primer strand in GT-pDNA until obtain the GT-dsDNA structure (Figure 1E and Supplementary Figure S2B). For this, different DNA substrates containing the GT mismatch located 8 nt (as in GT-pDNA) to 18 nt (as in GT-dsDNA) from the 3'-end were generated by adding 1 nt at a time at the 3'-OH terminus of the primer strand. Only GT-pDNAs with the GT mismatch located up to 13 nt far from the 3'-end induced a faster mobility of MutS (79-94% of protein in band a). MutS bound to the other GT-pDNAs exhibited a mobility similar to the DNA-unbound MutS or the MutS-GT-dsDNA complex. We also examined MutS migration on native gels in the presence of pDNAs containing all possible 12 mismatches (Figure 1F and Supplementary Figure S2C). Binding to pDNAs with CC, TC, GG and GA mismatches strongly induced a faster mobility of MutS since most of the protein-DNA complex migrated at ~331 kDa (82-99% of protein in band a). AC and CT mismatches produced a similar effect on MutS mobility, but to a lesser extent (35% and 28% of protein in band a, respectively). MutS bound to the other mismatches exhibited a migration similar to that observed for the matched pDNA (TG, AA, CA and TT) or free protein (AG).

To sum up, these data demonstrate that MutS binding to GT-pDNA provokes a faster migration of the protein relative to the DNA-unbound MutS on native gels. To induce this effect, the mismatched pDNA have to fulfill some important structural characteristics: a maximum separation of 13 nt between the mismatch and the 3'-OH terminus in the primer strand and the presence of a specific type of mismatch. On the other hand, GT-dsDNA, dsDNA and pDNA induce a retarded migration of the repair protein.

**MutS binding to mismatched replication DNA substrates induces a rearrangement of the protein structure**

Native electrophoretic mobility assays suggested that MutS undergoes a conformational change upon binding to mismatched pDNA structures, which could result in a tetramer to dimer transition or in a more compact protein structure. To determine if the interaction with GT-pDNA triggers a change in the oligomeric state of MutS, two dimeric MutS mutant versions, MutSR842E and MutSΔ798, were analyzed. In a previous report we showed that MutS from *P. aeruginosa* (855 amino acids) forms mainly tetramers in solution, and deletion of its C-terminal domain (Cter, 799-855 amino acids) or mutation at Arg 842 to Glu prevents its tetramerization (57). Native gel analysis revealed that the MutS-GT-pDNA complex (~331 kDa) migrated slower than DNA-unbound full-length MutSR842E (~193 kDa) (Supplementary Figure S3A). Moreover, MutSR842E bound to GT-pDNA showed an increased mobility relative to the uncomplexed protein as ~93% of the protein-DNA complex migrated at ~136 kDa (band a, Figure 2A and Supplementary Figure S3A). Association with GT-dsDNA, dsDNA or pDNA reduced the migration of MutSR842E (band c, Figure 2A and Supplementary Figure S3A). Most of the DNA-complexed MutSR842E migrated at ~316, 425 and 388-kDa, respectively. As observed for the wild type protein, GT-pDNA induced a fast mobility of MutSR842E when the GT mismatch was located up to 13 nt from the 3'-OH terminus (90-98% of protein in band a) (Figure 2B and Supplementary Figure S3B). Furthermore, pDNAs containing AC, CC, TC, GG, TG, CT, TT and GA triggered a faster mobility of MutSR842E, albeit to a lesser extent than GT (band a, Figure 2C and Supplementary Figure S3C). Truncated MutSΔ798 mutant bound to GT-pDNA also exhibited an increased mobility relative to the DNA-unbound protein whereas interaction with GT-dsDNA, dsDNA and pDNA slightly retarded its migration (Supplementary Figure S3A). These results clearly indicate that GT-pDNA has no effect on the oligomeric state of MutS as the MutS-GT-pDNA complex migrates slower than free MutSR842E and both tetrameric MutS and the dimeric mutants display a fast mobility upon binding to GT-pDNA.

We next examined if the binding to GT-pDNA changed the secondary and/or tertiary structures of MutS using far-UV circular dichroism (58)and limited trypsin proteolysis assays, respectively. The CD spectra of MutS in the absence or presence of DNA were recorded (Figure 2D and Supplementary Figure S3D), and used to estimate the fraction of secondary structures by the BeStSel web tool (48) (Figure 2E and Supplementary Figure S3E). MutS association with GT-pDNA reduced the disordered structure fraction and increased the α-helix content when compared

with free MutS. The other DNA substrates produced a similar effect on the secondary structure of MutS to that observed for GT-pDNA. Hence, MutS binding to DNA substrates induces further ordering of the secondary protein structure in a similar manner. In limited proteolysis experiments (Figure 2F), free MutS was readily cleaved by trypsin as ~22% of the full length protein was detected at the highest trypsin concentration used. DNA binding protected MutS from proteolysis. However, the MutS-GT-pDNA complex exhibited a higher resistance to proteolysis relative to MutS-GT-dsDNA as ~61% and ~33% of full length MutS was detected at the highest trypsin concentration, respectively. This result suggests that the mismatched replication substrate induces a rearrangement of the tertiary structure of MutS to a more compact conformation, which is less susceptible to tryptic digestion.

**MutS contains a novel putative DNA interaction site for DNA replication structures**

We hypothesized that the MutS conformational change induced by association with mismatched pDNAs arises from the interaction with novel protein residues. Several crystal structures of dimeric MutS have been published (59-61). All these structures show a similar arrangement of MutS (Figure 3A). The repair factor displays multiple domains arranged in the shape of a disk-like protein structure with two adjacent large channels. The heteroduplex DNA binds to the upper channel, in which the clamp domains of both monomers embrace the DNA helix and the mismatch-binding domain of only one subunit contacts mismatched bases. Within this domain, a Phe residue stacks with one of the mismatched bases and a Glu forms a hydrogen bond to the same base.

The presence of a novel DNA binding site in MutS was first evaluated using the web server BindUP (http://bindup.technion.ac.il/) (49), which predicts nucleic acid binding residues based on the electrostatic features of the three-dimensional (3D) protein surface. Because there is no a 3D-structure of *P. aeruginosa* MutS, we analyzed structures from *E. coli* MutS as the sequence homology between both proteins is 59%, indicating that they probably share at least 80% of the structure (57). Moreover, we determined that GT-pDNA also induced a higher mobility of *E. coli* MutS on native gels (Supplementary Figure S4A), which suggests that the conformational change induced by interaction with GT- pDNA is conserved between both bacterial MutS proteins. Using the high resolution 3D-structure of the full-length dimeric MutSD835R mutant from *E. coli* (PDB entry: 3ZLJ) solved in complex with a GT-dsDNA (62), three positive electrostatic surface patches were predicted by BindUP (Figure 3B and Supplementary Data). One of the predicted positive patches included residues from the clamp and mismatch-binding domains, highly overlapping with the identified mismatch binding interface (referred as DNA binding site I). The other predicted DNA binding surface consisted of amino acids from the ATPase, helix-turn-helix (HTH) and Cter domains. Residues present in the ATPase domain included His 760, which stacks the adenine nucleotide, and the catalytic amino acids Asn 616 and His 728 (59,63). It is possible that these residues were predicted to bind DNA because they are involved in the interaction with nucleotides. We next tested if the HTH and Cter domains are implicated in DNA binding. To examine this issue, the Cter domain alone or along with the contiguous HTH domain were fused to the maltose binding protein and then, both fusions were incubated with an excess of GT-pDNA, GT-dsDNA, pDNA or dsDNA (Supplementary Figure S4B). No binding was observed between fusions and DNA substrates since DNA-protein complexes were not detected under these conditions. This result could indicate that the HTH and Cter domains do not interact with DNA; however, further experiments are needed to establish this fact. Finally, the third positive surface included residues from the connector and core domains, which localize in the second channel (referred as DNA binding site II). This positive surface was also predicted to be a potential DNA binding site for crystal structures of all *E. coli* MutS, *Thermus aquaticus* MutS and human MutS$\alpha$ bound to a heteroduplex DNA (Supplementary Data).

In order to analyze the presence of a second DNA binding surface in MutS by other computational approach, we performed molecular docking simulations of the interaction between the *E. coli* MutS$\Delta$800 crystal structure (PDB entry: 1E3M) (59) and the modelled 3D-structure of DNA substrates using the HDOCK server (52). Docking of GT-dsDNA to the *E. coli* MutS$\Delta$800 structure showed that the most frequent DNA-MutS complex consisted in the GT-dsDNA bound to the DNA binding site I (Figure 3C and 3D, and Supplementary Table S1). In these docked structures, Phe 36 and Glu 38 were in close proximity (~12 Å) to the mismatched bases (Figure

3E). On the other hand, most of the docked *E. coli* MutSΔ800-GT-pDNA structures showed that GT-pDNA interacted with the DNA binding site II (Figure 3F and 3G, and Supplementary Table S1). The dsDNA region of GT-pDNA interacted with a coil-α-helix-coil (Arg 163-Glu 177) and a loop (Gln 281-Gly 285) present in the connector and core domains, respectively; and the single-stranded DNA template contacted connector residues (Glu 182-Gly 195) (Figure 3H). Interestingly, a second α helix (Ala 271-Glu 278) contacted GT-pDNA, wherein Arg 275 appeared to directly bind to the 3'-OH terminus (Figure 3I). All these residues always belonged to one of the two MutS monomers, similarly to the asymmetry in mismatch binding at the DNA binding site I. In the *E. coli* MutSΔ800-GT-pDNA structure, the mismatched bases did not interact with any protein residue (Figure 3G and 3H). The dsDNA structure was predicted to bind to both DNA binding sites while pDNA exclusively docked in the DNA binding site II (Supplementary Figures S4C and S4D, and Table S1). Finally, a single-stranded DNA, corresponding to the template strand, was not capable to bind to neither DNA binding site I nor site II (Supplementary Figure S4E and Table S1).

To sum up, our bioinformatics data provide support for a novel DNA binding surface located in the second channel of MutS, which may be involved in the specific association with replication DNA structures. Within this new binding site, an Arg residue (Arg 275 in *E. coli* MutS and Arg 272 in *P. aeruginosa* MutS) may directly contact the 3'-OH terminus of the primer strand. The conservation analysis using the ConSurf server (64) categorized this residue as highly conserved, with a score of 8, suggesting that it plays a critical role in the MutS function.

**Mutation of Arg 272 in MutS alters DNA-binding and ATPase activities, and is associated with a defective antimutagenic activity *in vivo***

Based on our data, Arg 272 in *P. aeruginosa* MutS could be implicated in the interaction with replication DNA structures. To address the role of this residue in the function of MutS, we carried out the biochemical and genetic analysis of the MutSR272E mutant version, in which the positive Arg 272 residue was replaced by the negative Glu amino acid. We also characterized MutSF33A, a mutant version of the mismatch binding Phe located at the DNA binding site I. Docking assays of MutSR272E showed no binding of GT-pDNA to the DNA binding site II (Supplementary Table S1). MutSR272E was not capable of interacting with GT-pDNA and GT-dsDNA in the Biacore flow system (Figure 4A and 4B). This mutant exhibited a decreased affinity for GT-pDNA, GT-dsDNA and pDNA in the EMSA assays, displaying a 7-, 6- and 2-fold lower binding, respectively (Supplementary Figures S1C to S1E). Conversely, substitution of Arg for Glu increased the affinity for dsDNA by 4-fold (Supplementary Figure S1F). The mismatch binding site I mutant, MutSF33A, did not associate with GT-pDNA and GT-dsDNA immobilized on a chip surface (Figure 4C and 4D). These results indicate that the R272E mutation renders MutS impaired for binding to GT-pDNA, GT-dsDNA and pDNA, whereas this change increases the MutS affinity for dsDNA.

To ascertain whether R272E and F33A mutations affect ATP hydrolysis by MutS, the ATPase activity of wild-type and mutant MutS proteins was assessed in parallel by quantifying the free phosphate released as a function of protein concentrations (Figure 4E). MutSR272E and MutSF33A showed a diminished ability to hydrolyze ATP compared to MutS, as both mutants released 2-fold lower amounts of phosphate at the highest protein concentration. We also tested the interaction of MutS mutants with MutL and β clamp by dot far-western blotting analysis (Supplementary Figure S5). MutSR272E and MutSF33A exhibited a similar affinity for MutL and β clamp than MutS. From these data, we conclude that R272E and F33A mutations diminish the ability of MutS to hydrolyze ATP, but have no effect on the association of MutS with the MMR and replication factors.

In order to analyze the *in vivo* antimutagenic activity of MutS mutants, we performed complementation assays by introducing plasmids bearing the wild-type and mutant *mutS* alleles into a *mutS*-deficient PAO1 strain (Figure 4F). Spontaneous mutations in different target genes on the *P. aeruginosa* chromosome were measured by estimating mutation rates to resistance to ciprofloxacin ($Cip^r$), rifampicin ($Rif^r$) and amikacin ($Amk^r$). Cells expressing MutSR272E showed increased mutation rates, which were 79-, 50- and 65-fold higher than that of transformants expressing MutS in the Rif, Cip and Amk resistance assays, respectively. Likewise, cells expressing MutSF33A displayed 54-, 96- and 23-fold higher mutation rates to $Cip^r$, $Rif^r$ and $Amk^r$, respectively. Control cells harboring the empty plasmid exhibited 306-, 196- and 251-fold increased

levels of mutations. These results indicate that MutSR272E and MutSF33A are partially impaired in its ability to revert replication errors. It is important to note that our mutation assay does not allow us to discriminate which mechanism is failing, MMR or control of Pol IV.

All together these data demonstrate that a single amino acid substitution at Arg 272 has a profound effect on DNA binding and ATP hydrolysis by *P. aeruginosa* MutS. A similar effect is observed when the mismatch binding Phe 33 residue is changed to Ala. It is important to note that these mutations do not alter the secondary and quaternary structure of the protein. Circular dichroism spectra of MutSR272E and MutSF33A were essentially unchanged from that of wild-type protein, and both mutants formed mainly tetramers as MutS (data not shown). Thus, both mutations affect DNA binding and ATP hydrolysis directly rather than altering the native conformation of the protein. In addition, our data demonstrate that both residues play a key role in the MutS antimutagenic activity *in vivo*.

**MutS remains associated with replication DNA structures containing a mismatch in the presence of ATP**

An important step in the MMR pathway is the exchange of ADP for ATP by MutS upon mismatch binding and the subsequent formation of an ATP-bound MutS sliding clamp on dsDNA that moves away from the mismatch. This sliding clamp state has been detected in biochemical assays. MutS slides off short double-stranded oligonucleotides in the presence of ATP while it remains bound to oligonucleotides with blocked ends (6,9,65). To test the ability of MutS to dissociate from GT-pDNA in the presence of ATP, we performed SPR assays in which MutS was bound to DNA and then, buffer alone and subsequently buffer containing ATP was flowed over the surface (Figure 5A and 5B). In these SPR experiments, DNA oligonucleotides were immobilized to a streptavidin-derivatized sensor chip via a single terminal biotin located at the dsDNA region. Thus, DNA substrates had a single blocked end. MutS readily associated with GT-pDNA and GT-dsDNA. Nevertheless, when the MutS-DNA complexes were challenged with ATP, MutS effectively dissociated from GT-dsDNA while it remained bound to GT-pDNA. Injection of buffer alone or amended with ATP to the MutS-GT-pDNA complex resulted in a very slight decrease in signals (~10 RU). Sensorgrams for MutS associated with GT-dsDNA showed a significant signal drop (~215 RU) when ATP was injected, while the MutS-GT-dsDNA complex was stable to buffer replacement (~25 RU). As a control, when MutS premixed with ATP was injected to these DNA-conjugated chips, MutS was not able to interact with GT-pDNA and GT-dsDNA (data not shown).

We further analyzed the ATP-induced MutS dissociation from DNA oligonucleotides with free ends (Supplementary Figure S6). For this, MutS was prebound to DNA oligonucleotides with both free ends and then nucleotides were added to the reaction. Reaction products were analyzed in native gels and the free DNA fraction was calculated. The repair protein was not released from GT-pDNA upon the addition of nucleotides. The free DNA fraction was ~3% and ~4% in the presence of ATP and ADP, respectively, whereas it represented ~1% in the free nucleotide reaction. ATP induced MutS dissociation from pDNA, GT-dsDNA and dsDNA as revealed by the higher fraction of free DNA (32%, 51%, 53%) relative to that observed when reactions contained ADP (15%, 9%, 23%) or no nucleotide was added (11%, 6%, 15%). All these results clearly establish that the MutS-GT-pDNA complex is resistant to dissociation upon ATP challenge while MutS is prone to release from the other DNA structures when exposed to ATP.

It has been well documented that the ATPase activity of MutS is stimulated by mismatched or matched dsDNAs with free ends as MutS dissociates from DNA upon ATP binding, increasing ATP hydrolysis (9,65,66). Hence, it can be predicted that GT-pDNA should not stimulate ATP hydrolysis by MutS whereas the other DNA substrates should promote the ATPase activity. We investigated the effect of DNA substrates on the ATPase activity of MutS by measuring ATP hydrolysis in the absence or presence of a fixed concentration of DNA oligonucleotides with free ends and increasing ATP concentrations (Figure 5C and 5D). Hydrolysis of ATP by MutS was increased as ATP was titrated into the reaction. The ATPase activity was completely inhibited by GT-pDNA at low ATP concentrations (3-50 µM) whereas this DNA substrate had no effect at 100 and 200 µM ATP. At the highest ATP concentration (400 µM), GT-pDNA increased the ATP hydrolysis by ~1.5-fold. GT-dsDNA and pDNA stimulated the ATPase activity at 200 and 400 µM ATP (~1.4-fold) while dsDNA only increased this activity at 400 µM (~1.2-fold). The experiments described above

demonstrate that GT-pDNA has a dual effect on the ATPase activity of MutS: it can inhibit or stimulate ATP hydrolysis depending on the ATP concentration. pDNA, like the MMR substrates, is able to increase the ATPase activity of MutS.

**MutS interaction with MutL is modulated by the replication GT-pDNA structure**

Interaction between *P. aeruginosa* MutS and MutL has not previously been examined in detail. Therefore, we evaluated the association of MutS with MutL by SPR (Supplementary Figure S7A). MutS specifically bound to MutL immobilized on a chip surface. Nevertheless, it was not possible to accurately determine the kinetic and equilibrium constants since MutS did not dissociate from immobilized MutL. We further examined this interaction by dot far-Western blotting analysis (Figure 6A). Binding of soluble MutS to MutL immobilized on nitrocellulose was detected at all tested amounts, and sharply increased between 3 and 12 pmol of MutL. A similar result was obtained for the interaction between soluble MutS and immobilized β clamp; however, the intensities were higher (~3-fold) for MutL spots than for β clamp spots. We next asked if the DNA substrates affect the MutS-MutL association. To examine this issue, preformed MutS-DNA complexes were spotted on nitrocellulose and then incubated with soluble MutL (Figure 6B and Supplementary Figure S7B). Interaction of MutL with MutS-GT-pDNA was reduced, as shown by the ~2-fold decrease in the intensity of spots (3 and 6 pmol) compared to the control without DNA. The other DNA substrates did not display a significant effect on the strength of the MutS-MutL interaction. These data further support the conclusion that the binding affinity of MutS for MutL is higher than that of MutS for β clamp, and GT-pDNA specifically modulates binding of MutS to MutL.

**MutL endonuclease activity is stimulated by MutS but not by β clamp**

It has been reported that *P. aeruginosa* MutL displays a non-specific nicking endonuclease activity dependent on $Mg^{+2}$ and $Mn^{+2}$, which is required for MMR (67,68). This endonuclease activity has been evidenced by the ability of MutL to incise supercoiled plasmids and linear dsDNA substrates. We investigated if MutL is capable of nicking replication DNA substrates by incubating DNA oligonucleotides in the presence of increasing MutL concentrations (Figure 6C). Reactions were analyzed on native gels to quantify the amount of uncleaved DNA. MutL was able to incise GT-pDNA and GT-dsDNA as the quantity of both DNA substrates decreased with increased MutL concentrations. This enzyme appeared to have a slight preference for the mismatched dsDNA. Almost all GT-dsDNA was cleaved at the highest MutL amount whereas a ~38% of GT-pDNA remained uncleaved. MutL activity was completely inhibited in control reactions containing the divalent ion-chelating compound EDTA. MutL also incised the matched pDNA and dsDNA (Supplementary Figure S7C), confirming its mismatch-independent activity. As previous works reported that MutL endonuclease activity is enhanced by MutS or β clamp (15,17-21), we tested the effect of both factors on the nicking activity of MutL (Figure 6D). For this, GT-pDNA and GT-dsDNA were individually mixed with a low concentration of MutL and stoichiometric amounts of MutS or β clamp. No detectable activity was observed in reactions with MutL alone (~93% and ~95% of uncleaved GT-pDNA and GT-dsDNA, respectively). Addition of MutS stimulated the endonuclease activity of MutL as ~61% and ~52% of GT-pDNA and GT-dsDNA remained uncleaved, respectively. In the presence of β clamp, ~97% and ~89% of uncleaved GT-pDNA and GT-dsDNA was observed, respectively, showing that the replication factor had no effect on the MutL nicking activity. It has been demonstrated that stimulation of MutL activity by processivity factors is dependent on the physical interaction between both proteins (69,70). When the formation of the MutL-β clamp complex was examined by injecting β clamp over MutL immobilized to a chip surface, no binding was observed (Supplementary Figure S7D). A similar result was obtained by dot far-Western blotting (data not shown). These findings demonstrate that MutL is able to cleave replication and MMR substrates in a mismatch-independent manner, activity that is enhanced by MutS but not by β clamp.

## DISCUSSION

Most of the biochemical studies characterizing MutS activities have been carried out with double-stranded DNA (dsDNA), the substrate of the mismatch repair process. In the current work, and for the first time to our knowledge, it has been performed a detailed analysis of the interaction of MutS with DNA replication substrates and their effect on the different activities displayed by the repair factor. Our data clearly demonstrated that MutS from *P. aeruginosa* is able to interact with DNA replication structures, primed DNA (pDNA), containing or not mismatched bases. Binding affinities of MutS to mismatched and matched pDNA were comparable to that observed for the mismatched dsDNA, following the order: GT-pDNA > GT-dsDNA > pDNA. Notably, MutS binding to GT-pDNA and GT-dsDNA displayed different kinetic behaviors. MutS association with mismatched dsDNA followed a single-site-binding model. Kinetic data for MutS binding to mismatched pDNA did not fit to models that take into account the presence of a single-binding site or two-binding sites, including or not a conformational change. This poor overlap of models with SPR kinetic data could reflect a very complex process of DNA binding in which two binding sites contribute differently to the global binding kinetics, in addition to different conformational changes upon binding each site. Moreover, the dimer-tetramer equilibrium should be taken into account (62). Additional studies will be required to establish a proper binding model for the MutS interaction with mismatched DNA replication structures.

Current data describe a unique DNA interaction site in the disk-like MutS repair factor. This interaction surface located in the upper channel (referred in this work as DNA binding site I) specifically binds to mismatched dsDNA (59-61). Two highly conserved residues, Phe and Glu, in the mismatch binding domain directly contact the mismatched bases. Our bioinformatics analysis predicted a novel DNA interaction surface (named DNA binding site II) for pDNA, which encompassed residues from the connector and core domains positioned in the lower channel of MutS. Among these residues, a highly conserved Arg on an exposed α helix of the core domain appeared to directly interact with the 3'-OH terminus of the pDNA. Substitution of Glu for Arg 272 in *P. aeruginosa* MutS (MutSR272E mutant) conferred a specific defect in mismatch binding. MutSR272E exhibited a decreased binding affinity for mismatched pDNA and dsDNA substrates compared to the wild-type protein. Conversely, association with pDNA was slightly reduced whereas binding to dsDNA was increased in this mutant version. Thus, the Arg 272 to Glu change resulted in a lower affinity of MutS for mismatched DNA relative to matched substrates, decreasing the mismatch discriminatory capacity of MutS. Mutating Phe 33 to Ala in *P. aeruginosa* MutS (MutSF33A mutant) also provoked a defect in mismatch binding as MutSF33A showed no interaction with mismatched pDNA and dsDNA. Defects in mismatch discrimination have been previously described for mismatch binding mutants in other bacterial MutS and eukaryotic MutSα. Ala substitution at Phe severely impairs interaction with mismatched dsDNA and, to a lesser extent, with matched dsDNA, resulting in a similar residual affinity for both substrates (71,72). Changes in the Glu residue slightly affect mismatch interaction but enhance association with dsDNA and consequently, binding affinities for unpaired and paired dsDNA become comparable (73-75). Therefore, our findings suggest a common outcome of mutations in both DNA binding sites, which is the impairment of the MutS ability to discriminate mismatches. Other defect associated with R272E and F33A mutations corresponded to a reduced ATPase activity of *P. aeruginosa* MutS. MutSR272E and MutSF33A displayed a decreased ATP hydrolysis, which was ~2-fold lower than that observed for wild-type MutS. This defect has not been shown for mismatch binding mutants of other MutS proteins, in which mutation of Phe or Glu has no effect on basal ATPase levels (71,73,74,76,77). It is possible to speculate that there is a strong communication between DNA interaction and ATPase sites in *P. aeruginosa* MutS, since mutation of the DNA binding Phe and Arg residues affects the overall ATPase activity of the repair factor. Finally, single amino acid substitution at Arg 272, as well as at Phe 33, resulted in a noticeable defect in the MutS antimutagenic activity. MutSR272E and MutSF33A mutants failed to fully complement a MutS-deficient strain. We assume that this defect is due to a reduced DNA binding ability and not to an impaired ATPase activity as oligomeric MutS mutants, MutSΔ798 and MutSR842E, show a similar ATPase defect but are completely proficient for mismatch correction *in vivo* (57). It is interesting to note that the strong DNA binding defect displayed by MutSR272E and MutSF33A did not correlate

with the partial reduction of their antimutagenic capacity. This feature has been also shown for *E. coli* and *Saccharomyces cerevisiae* MutS mutants in the mismatch binding Glu residue (73,74,78). Nevertheless, and unlike *P. aeruginosa* MutSF33A, Phe mutants of MutS from other organisms show an almost complete loss of the repair activity (73,76,79,80). These data strongly suggest that *P. aeruginosa* MutS relies on additional residues or other factors to verify binding to mismatched DNA. Taking together, our findings demonstrate that the highly conserved Arg 272 corresponds to a novel DNA binding residue in MutS, which plays an important role in the correction of replication errors.

Essential features of MutS for effective MMR initiation are its large conformational changes upon binding to cofactors, mismatched dsDNA and nucleotides, and a robust allosteric signaling between the ATPase site and the DNA binding site I (4,5). In the absence of DNA, clamp domains of ADP-bound MutS are in a dynamic open/close equilibrium that allows DNA to enter the MutS dimer (60,81,82). Loading of MutS onto homoduplex DNA stabilizes a closed state of clamp domains while DNA binding domains adopt a relatively open conformation that allows searching for mismatches (60,83). Upon mismatch recognition, DNA binding domains move toward each other allowing specific contacts of Phe and Glu with mismatched bases, which promotes the exchange of ADP for ATP and formation of a sliding clamp on DNA (7,9,59-61,83,84). In this conformation, clamp domains cross each other and mismatch binding and connector domains reorganize, pushing the DNA downward into a novel channel and generating a new binding site for MutL (10). In this work, we provide evidences of a different conformational change of MutS triggered by binding to mismatched pDNA. The repair protein appeared to adopt a more compact conformation by reorganizing its tertiary structure. This new state was revealed as a fast-migrating MutS-DNA complex on native gels, which exhibited a high resistance to proteolysis. We discarded that binding to mismatched pDNA induces a specific rearrangement of the secondary structure or a change in the oligomeric state of MutS. The presence of mismatched pDNA conferred MutS with a more ordered secondary structure, an effect produced by all DNA substrates evaluated. In addition, dimeric MutSR842E and MutSΔ798 mutants showed an increased mobility when bound to mismatched pDNA, demonstrating that this DNA structure induces a protein compaction of the MutS dimer and tetramer. Understanding how MutS adopts this novel conformation remains to be elucidated. However, it is possible to postulate that the new MutS structure represents a state wherein both DNA binding sites are occupied in the dimer, the DNA binding site I by the mismatch and the DNA binding site II by the 3'-OH terminus. Both DNA interaction surfaces are distant as Arg 275 is located ~50 Å far from Phe 36 in *E. coli* MutS structures. Thus, and taking into account that the distance between the mismatch and the 3'-OH terminus required to induce the MutS compaction was ~27-44 Å (8-13 nt), DNA binding sites I and II should approach each other, resulting in a more compact MutS conformation. An interesting question is in what way MutS accesses to mismatched pDNA in the cellular context. This DNA structure is present at replication forks, where a mismatch is located close to a primer-template junction occupied by a β clamp molecule. Under this scenario, MutS should gain access to the 3'-OH terminus from β clamp. In this regard, *in vitro* studies demonstrated that processivity factors can release the primer-template junction and diffuse along the single-stranded template DNA (85,86). Accordingly, it is tempting to speculate that when MutS transiently associated with the replication machinery binds to a mismatch, the repair factor interacts with the 3'-OH terminus by displacing β clamp from the primed site to the single-stranded region. Once MutS accesses to the 3'-OH terminus, this factor efficiently associates with β clamp as binding affinity is increased in the presence of mismatched pDNA (26).

A hallmark of the mismatch repair process is the ATP induced transition of MutS from a stationary clamp bound to a mismatch to a mobile sliding clamp (6,9-11). A similar molecular mechanism underlines MutS function in the inhibition of recombination between divergent sequences as initial mismatch recognition and sliding clamp formation by MutS also play an important role in heteroduplex rejection (55,56). Our data indicated that MutS remains associated with mismatched pDNA upon challenge with ATP. Conversely, ATP promoted MutS release from pDNA and dsDNA, containing or not a mismatch. One possibility to explain this unusual MutS behavior is that interaction of the repair factor with mismatched pDNA prevents the exchange of ADP for ATP. Indeed, this DNA substrate inhibited ATP hydrolysis by MutS in an ATP concentration-dependent manner. ATPase activity was only detected at ATP concentrations in the

100-400 μM range. This observation is consistent with the idea that MutS association with mismatched pDNA decreases its binding affinity for ATP and thus, ATP hydrolysis is abolished at low ATP amounts. Inhibition of ATP hydrolysis was not observed for the other DNA substrates, including pDNA, which indicates that interaction with both DNA binding sites of MutS is critical for ATPase inhibition. This fact also reveals a strong allosteric signaling between three active sites: the ATPase site and DNA binding sites I and II. On the other hand, our experiments showed that the MutS-mismatched pDNA complex is highly stable even in the presence of 5 mM ATP, a condition in which exchange of ADP for ATP is expected to occur. It suggests that ATP-bound MutS is not able to slide on this replication DNA structure, which may result from an inability of MutS to adopt the sliding clamp conformation when both DNA binding sites are occupied. Notably, MutS interaction with mismatched replication DNA structures limits the exchange of ADP for ATP and the conformational transition into a sliding clamp, favoring MutS function in the regulation of Pol IV access to replication sites instead in MMR.

Another critical step for correcting mismatches is the MutS-MutL interaction at early stages of MMR. Our data showed that *P. aeruginosa* MutS binds to MutL with high affinity. This interaction was modulated by the mismatched pDNA substrate while no effect was observed by the other DNA structures. The mismatched pDNA decreased MutS affinity for MutL, indicating that the MutS-MutL interaction is unfavorable when a mismatch is close to a primed site. This effect may be due to the MutL interaction surface is not exposed in the conformation adopted by MutS when both DNA binding sites are occupied. A surface exposed region involving Gln 212 and Gln 213 in *E. coli* MutS is essential for interaction with MutL while Phe 319 and Phe 320 residues in *Bacillus subtilis* MutS are important for the MutS-MutL interaction (87,88). Gln 212 and Gln 213 residues, but not Phe 319 and Phe 320, are conserved in *P. aeruginosa* MutS. Both Gln residues are close to the DNA binding residue, Arg 272, suggesting that MutL binding residues may be occluded when DNA binding sites I and II approach each other upon binding mismatched pDNA (Supplementary Figure S4F). On the other hand, association of the repair factor with β clamp is involved in the control of Pol IV mutagenesis in *P. aeruginosa* cells (26). Our previous data showed that *P. aeruginosa* MutS interacts with β clamp *via* the $^{816}$QSDLF$^{820}$ binding site (36). Strikingly, MutS association with β clamp is enhanced in the presence of mismatched pDNA (26), again highlighting a regulatory effect of this DNA structure on MutS interaction with a partner. As mismatched pDNA induce a large conformational change in MutS, it is possible to assume that interaction with β clamp is favored in this MutS structural state. In the MMR pathway, the major MutS conformational change corresponds to the formation of a sliding clamp upon ATP binding (10). Interesting, under this conformation, the DNA binding Arg residue is occluded inside the clamp (Supplementary Figures S4G and S4H). All these data together reveal that MutS interaction with a particular DNA structure favors association with β clamp or MutL, probably by adopting a specific conformation, and thus, contributes to pathway choice.

In *P. aeruginosa*, the *mutS*, *mutL* and *uvrD* genes are present; however, MutH and Dam homologues have not been identified and dGATC methylation has not been detected in this bacterium (89). *P. aeruginosa* MutS binds to β clamp and this interaction plays a role in regulating Pol IV access to replication sites but not in MMR (26,36). MutS from other organisms also interacts with processivity factors. Nevertheless, a limited contribution of this association in the MMR has been observed as disruption of the β clamp binding motif in MutS results in a modest repair defect (38-40,90). In addition, *P. aeruginosa* MutL exhibits an endonuclease activity that appears to be essential for MMR (67,68). This enzyme shows a metal ion-dependent activity that nicks closed or lineal dsDNA with any sequence specificity. Our results indicated that MutL incises mismatched and matched pDNA and dsDNA with a similar efficiency, indicating that there is not a strong preference for the MMR substrate. The MutL nicking activity was only stimulated by MutS. The effect of protein factors on the endonuclease activity of MutL has been previously determined. MutSα and PCNA directly activate MutLα endonuclease in human and yeast (17-19,21). The nicking activity of *T. thermophilus* MutL is strongly stimulated by MutS; however β clamp does not influence this activity (20). Conversely, endonuclease activity of *B. subtilis* MutL is enhanced by β clamp (91). Direct MutL association with processivity factors is critical for stimulation of its endonuclease activity and MMR (69,91). In *P. aeruginosa*, β clamp had no effect on the MutL

endonuclease activity, which correlated with a residual interaction between both factors, albeit MutL contains a β clamp-interacting motif ($^{492}$QPLLVP$^{497}$). In addition, we have previously found that *P. aeruginosa* β clamp inhibits the assembly of the MutS-MutL complex; an effect does not displayed by the MutS mutant in the β clamp binding site, MutS$^{\beta}$ (26). Similarly, human PCNA competes with MutLα for binding to MutSβ as both factors share the same interaction surface on MutSβ (92). As *P. aeruginosa* MutS$^{\beta}$ interacts with MutL to the same extent as MutS (26), β clamp inhibition of the MutS-MutL association does not involve a competition for the same site on MutS. Finally, and taking into account that β clamp has no role in the stimulation of the MutL endonuclease activity and this factor hampers MutL binding to MutS, MutL action is expected to take place at β clamp free zones on the *P. aeruginosa* chromosome. Microscopy studies showed that β clamp molecules accumulate behind replication forks forming clamp zones in living cells (30,31). Therefore, it is conceivable that repair reactions occur at distant sites from the replication machinery, which is consistent with the fact that active sites of repair do not colocalize with replisome components in cells (32). This has an important implication for the MMR mechanism of *P. aeruginosa* since DNA replication-associated signals can not be used for strand discrimination. Remarkably, our data suggest that the Dam/MutH-independent MMR from *P. aeruginosa* is uncoupled from DNA replication.

According to our findings and previous data we propose the following model for the RPS/MMR decision (Figure 7): (A) (1) ADP-bound MutS dynamically opens and closes its clamp domains, allowing MutS to load on DNA; (B) In the RSP pathway, ADP-bound MutS is transiently associated with the replication machinery. When the repair factor recognizes a mismatch located near to β clamp (β clamp zone), MutS closes its clamp domains and Phe and Glu residues in the DNA binding site I contact the mismatch; (C) MutS displaces β clamp from the primed site to the single-stranded region, which facilitates MutS interaction with the 3'-OH terminus through the Arg residue in the DNA binding site II; (D) MutS is prone to adopt a more compact conformation that efficiently associates with β clamp, resulting in Pol IV dissociation from the processivity factor and subsequent excision of the incorrect nucleotide. Under this structural state, MutS remains bound to ADP and can not adopt a sliding clamp conformation as well as the repair protein decreases its affinity for MutL, assuring that the repair reaction is not initiated; (B´) In the MMR pathway, MutS binds to a mismatch in a β clamp free zone located far from the replication machinery; (C´) MutS mismatch binding triggers the exchange of ADP for ATP and the conformational change into a sliding clamp; (D´) ATP-bound MutS sliding clamp physically interacts with MutL, activating downstream steps of the repair process.

In conclusion, the present work sheds light on factors influencing the mismatch repair/control of specialized DNA polymerases pathway choice, which include MutS interaction with different protein partners and DNA structures, the nucleotide-bound MutS state and specific conformational changes**.**

**FUNDING**

This work was supported by grants from Consejo Nacional de Investigaciones Científicas y Técnicas [PIP 20130100360]; Secretaría de Ciencia y Tecnología de la Universidad Nacional de Córdoba [33620180101008CB]; and Agencia Nacional de Promoción Científica y Técnica [PICT 2017-1857].

## REFERENCES


1. Liu, D., Keijzers, G. and Rasmussen, L.J. (2017) DNA mismatch repair and its many roles in eukaryotic cells. *Mutat Res*, **773**, 174-187.
2. Baretti, M. and Le, D.T. (2018) DNA mismatch repair in cancer. *Pharmacology & therapeutics*, **189**, 45-62.
3. Lenhart, J.S., Pillon, M.C., Guarne, A., Biteen, J.S. and Simmons, L.A. (2016) Mismatch repair in Gram-positive bacteria. *Res Microbiol*, **167**, 4-12.
4. Groothuizen, F.S. and Sixma, T.K. (2016) The conserved molecular machinery in DNA mismatch repair enzyme structures. *DNA Repair (Amst)*, **38**, 14-23.
5. Hingorani, M.M. (2016) Mismatch binding, ADP-ATP exchange and intramolecular signaling during mismatch repair. *DNA Repair (Amst)*, **38**, 24-31.
6. Acharya, S., Foster, P.L., Brooks, P. and Fishel, R. (2003) The coordinated functions of the E. coli MutS and MutL proteins in mismatch repair. *Mol Cell*, **12**, 233-246.
7. Cho, W.K., Jeong, C., Kim, D., Chang, M., Song, K.M., Hanne, J., Ban, C., Fishel, R. and Lee, J.B. (2012) ATP alters the diffusion mechanics of MutS on mismatched DNA. *Structure*, **20**, 1264-1274.
8. Gorman, J., Wang, F., Redding, S., Plys, A.J., Fazio, T., Wind, S., Alani, E.E. and Greene, E.C. (2012) Single-molecule imaging reveals target-search mechanisms during DNA mismatch repair. *Proc Natl Acad Sci U S A*, **109**, E3074-3083.
9. Gradia, S., Subramanian, D., Wilson, T., Acharya, S., Makhov, A., Griffith, J. and Fishel, R. (1999) hMSH2-hMSH6 forms a hydrolysis-independent sliding clamp on mismatched DNA. *Mol Cell*, **3**, 255-261.
10. Groothuizen, F.S., Winkler, I., Cristovao, M., Fish, A., Winterwerp, H.H., Reumer, A., Marx, A.D., Hermans, N., Nicholls, R.A., Murshudov, G.N. *et al.* (2015) MutS/MutL crystal structure reveals that the MutS sliding clamp loads MutL onto DNA. *Elife*, **4**, e06744.
11. Liu, J., Hanne, J., Britton, B.M., Bennett, J., Kim, D., Lee, J.B. and Fishel, R. (2016) Cascading MutS and MutL sliding clamps control DNA diffusion to activate mismatch repair. *Nature*, **539**, 583-587.
12. Glickman, B.W. and Radman, M. (1980) Escherichia coli mutator mutants deficient in methylation-instructed DNA mismatch correction. *Proc Natl Acad Sci U S A*, **77**, 1063-1067.
13. Burdett, V., Baitinger, C., Viswanathan, M., Lovett, S.T. and Modrich, P. (2001) In vivo requirement for RecJ, ExoVII, ExoI, and ExoX in methyl-directed mismatch repair. *Proc Natl Acad Sci U S A*, **98**, 6765-6770.
14. Dao, V. and Modrich, P. (1998) Mismatch-, MutS-, MutL-, and helicase II-dependent unwinding from the single-strand break of an incised heteroduplex. *J Biol Chem*, **273**, 9202-9207.
15. Liu, J., Lee, R., Britton, B.M., London, J.A., Yang, K., Hanne, J., Lee, J.B. and Fishel, R. (2019) MutL sliding clamps coordinate exonuclease-independent Escherichia coli mismatch repair. *Nat Commun*, **10**, 5294.
16. Kadyrova, L.Y. and Kadyrov, F.A. (2016) Endonuclease activities of MutLalpha and its homologs in DNA mismatch repair. *DNA Repair (Amst)*, **38**, 42-49.
17. Kadyrov, F.A., Dzantiev, L., Constantin, N. and Modrich, P. (2006) Endonucleolytic function of MutLalpha in human mismatch repair. *Cell*, **126**, 297-308.
18. Kadyrov, F.A., Holmes, S.F., Arana, M.E., Lukianova, O.A., O'Donnell, M., Kunkel, T.A. and Modrich, P. (2007) Saccharomyces cerevisiae MutLalpha is a mismatch repair endonuclease. *J Biol Chem*, **282**, 37181-37190.
19. Pluciennik, A., Dzantiev, L., Iyer, R.R., Constantin, N., Kadyrov, F.A. and Modrich, P. (2010) PCNA function in the activation and strand direction of MutLalpha endonuclease in mismatch repair. *Proc Natl Acad Sci U S A*, **107**, 16066-16071.
20. Shimada, A., Kawasoe, Y., Hata, Y., Takahashi, T.S., Masui, R., Kuramitsu, S. and Fukui, K. (2013) MutS stimulates the endonuclease activity of MutL in an ATP-hydrolysis-dependent manner. *FEBS J*, **280**, 3467-3479.

21. Smith, C.E., Bowen, N., Graham, W.J.t., Goellner, E.M., Srivatsan, A. and Kolodner, R.D. (2015) Activation of Saccharomyces cerevisiae Mlh1-Pms1 Endonuclease in a Reconstituted Mismatch Repair System. *J Biol Chem*, **290**, 21580-21590.
22. Ghodgaonkar, M.M., Lazzaro, F., Olivera-Pimentel, M., Artola-Boran, M., Cejka, P., Reijns, M.A., Jackson, A.P., Plevani, P., Muzi-Falconi, M. and Jiricny, J. (2013) Ribonucleotides misincorporated into DNA act as strand-discrimination signals in eukaryotic mismatch repair. *Mol Cell*, **50**, 323-332.
23. Lujan, S.A., Williams, J.S., Clausen, A.R., Clark, A.B. and Kunkel, T.A. (2013) Ribonucleotides are signals for mismatch repair of leading-strand replication errors. *Mol Cell*, **50**, 437-443.
24. Yao, N.Y., Schroeder, J.W., Yurieva, O., Simmons, L.A. and O'Donnell, M.E. (2013) Cost of rNTP/dNTP pool imbalance at the replication fork. *Proc Natl Acad Sci U S A*, **110**, 12942-12947.
25. Henrikus, S.S., van Oijen, A.M. and Robinson, A. (2018) Specialised DNA polymerases in Escherichia coli: roles within multiple pathways. *Curr Genet*, **64**, 1189-1196.
26. Margara, L.M., Fernandez, M.M., Malchiodi, E.L., Argarana, C.E. and Monti, M.R. (2016) MutS regulates access of the error-prone DNA polymerase Pol IV to replication sites: a novel mechanism for maintaining replication fidelity. *Nucleic Acids Res*, **44**, 7700-7713.
27. Lenne-Samuel, N., Wagner, J., Etienne, H. and Fuchs, R.P. (2002) The processivity factor beta controls DNA polymerase IV traffic during spontaneous mutagenesis and translesion synthesis in vivo. *EMBO Rep*, **3**, 45-49.
28. Lv, L., Wang, F., Ma, X., Yang, Y., Wang, Z., Liu, H., Li, X., Liu, Z., Zhang, T., Huang, M. *et al.* (2013) Mismatch repair protein MSH2 regulates translesion DNA synthesis following exposure of cells to UV radiation. *Nucleic Acids Res*, **41**, 10312-10322.
29. Zlatanou, A., Despras, E., Braz-Petta, T., Boubakour-Azzouz, I., Pouvelle, C., Stewart, G.S., Nakajima, S., Yasui, A., Ishchenko, A.A. and Kannouche, P.L. (2011) The hMsh2-hMsh6 complex acts in concert with monoubiquitinated PCNA and Pol eta in response to oxidative DNA damage in human cells. *Mol Cell*, **43**, 649-662.
30. Moolman, M.C., Krishnan, S.T., Kerssemakers, J.W., van den Berg, A., Tulinski, P., Depken, M., Reyes-Lamothe, R., Sherratt, D.J. and Dekker, N.H. (2014) Slow unloading leads to DNA-bound beta2-sliding clamp accumulation in live Escherichia coli cells. *Nat Commun*, **5**, 5820.
31. Su'etsugu, M. and Errington, J. (2011) The replicase sliding clamp dynamically accumulates behind progressing replication forks in Bacillus subtilis cells. *Mol Cell*, **41**, 720-732.
32. Schmidt, T.T. and Hombauer, H. (2016) Visualization of mismatch repair complexes using fluorescence microscopy. *DNA Repair (Amst)*, **38**, 58-67.
33. Schroering, A.G., Edelbrock, M.A., Richards, T.J. and Williams, K.J. (2007) The cell cycle and DNA mismatch repair. *Exp Cell Res*, **313**, 292-304.
34. Klocko, A.D., Schroeder, J.W., Walsh, B.W., Lenhart, J.S., Evans, M.L. and Simmons, L.A. (2011) Mismatch repair causes the dynamic release of an essential DNA polymerase from the replication fork. *Mol Microbiol*, **82**, 648-663.
35. Lopez de Saro, F.J., Marinus, M.G., Modrich, P. and O'Donnell, M. (2006) The beta sliding clamp binds to multiple sites within MutL and MutS. *J Biol Chem*, **281**, 14340-14349.
36. Monti, M.R., Miguel, V., Borgogno, M.V. and Argarana, C.E. (2012) Functional analysis of the interaction between the mismatch repair protein MutS and the replication processivity factor beta clamp in Pseudomonas aeruginosa. *DNA Repair (Amst)*, **11**, 463-469.
37. Pillon, M.C., Miller, J.H. and Guarne, A. (2011) The endonuclease domain of MutL interacts with the beta sliding clamp. *DNA Repair (Amst)*, **10**, 87-93.
38. Pluciennik, A., Burdett, V., Lukianova, O., O'Donnell, M. and Modrich, P. (2009) Involvement of the beta clamp in methyl-directed mismatch repair in vitro. *J Biol Chem*, **284**, 32782-32791.
39. Shell, S.S., Putnam, C.D. and Kolodner, R.D. (2007) The N terminus of Saccharomyces cerevisiae Msh6 is an unstructured tether to PCNA. *Mol Cell*, **26**, 565-578.
40. Simmons, L.A., Davies, B.W., Grossman, A.D. and Walker, G.C. (2008) Beta clamp directs localization of mismatch repair in Bacillus subtilis. *Mol Cell*, **29**, 291-301.
41. Haye, J.E. and Gammie, A.E. (2015) The Eukaryotic Mismatch Recognition Complexes Track with the Replisome during DNA Synthesis. *PLoS Genet*, **11**, e1005719.

42. Liao, Y., Schroeder, J.W., Gao, B., Simmons, L.A. and Biteen, J.S. (2015) Single-molecule motions and interactions in live cells reveal target search dynamics in mismatch repair. *Proc Natl Acad Sci U S A*, **112**, E6898-6906.
43. Hombauer, H., Campbell, C.S., Smith, C.E., Desai, A. and Kolodner, R.D. (2011) Visualization of eukaryotic DNA mismatch repair reveals distinct recognition and repair intermediates. *Cell*, **147**, 1040-1053.
44. Kleczkowska, H.E., Marra, G., Lettieri, T. and Jiricny, J. (2001) hMSH3 and hMSH6 interact with PCNA and colocalize with it to replication foci. *Genes Dev*, **15**, 724-736.
45. Lenhart, J.S., Sharma, A., Hingorani, M.M. and Simmons, L.A. (2013) DnaN clamp zones provide a platform for spatiotemporal coupling of mismatch detection to DNA replication. *Mol Microbiol*, **87**, 553-568.
46. Elez, M., Murray, A.W., Bi, L.J., Zhang, X.E., Matic, I. and Radman, M. (2010) Seeing mutations in living cells. *Curr Biol*, **20**, 1432-1437.
47. Smith, B.T., Grossman, A.D. and Walker, G.C. (2001) Visualization of mismatch repair in bacterial cells. *Mol Cell*, **8**, 1197-1206.
48. Micsonai, A., Wien, F., Bulyaki, E., Kun, J., Moussong, E., Lee, Y.H., Goto, Y., Refregiers, M. and Kardos, J. (2018) BeStSel: a web server for accurate protein secondary structure prediction and fold recognition from the circular dichroism spectra. *Nucleic Acids Res*, **46**, W315-W322.
49. Paz, I., Kligun, E., Bengad, B. and Mandel-Gutfreund, Y. (2016) BindUP: a web server for non-homology-based prediction of DNA and RNA binding proteins. *Nucleic Acids Res*, **44**, W568-574.
50. Sim, A.Y., Minary, P. and Levitt, M. (2012) Modeling nucleic acids. *Current opinion in structural biology*, **22**, 273-278.
51. van Dijk, M. and Bonvin, A.M. (2009) 3D-DART: a DNA structure modelling server. *Nucleic Acids Res*, **37**, W235-239.
52. Yan, Y., Zhang, D., Zhou, P., Li, B. and Huang, S.Y. (2017) HDOCK: a web server for protein-protein and protein-DNA/RNA docking based on a hybrid strategy. *Nucleic Acids Res*, **45**, W365-W373.
53. Humphrey, W., Dalke, A. and Schulten, K. (1996) VMD: visual molecular dynamics. *J Mol Graph*, **14**, 33-38, 27-38.
54. Ehrat, E.A., Johnson, B.R., Williams, J.D., Borchert, G.M. and Larson, E.D. (2012) G-quadruplex recognition activities of E. Coli MutS. *BMC molecular biology*, **13**, 23.
55. Honda, M., Okuno, Y., Hengel, S.R., Martin-Lopez, J.V., Cook, C.P., Amunugama, R., Soukup, R.J., Subramanyam, S., Fishel, R. and Spies, M. (2014) Mismatch repair protein hMSH2-hMSH6 recognizes mismatches and forms sliding clamps within a D-loop recombination intermediate. *Proc Natl Acad Sci U S A*, **111**, E316-325.
56. Snowden, T., Acharya, S., Butz, C., Berardini, M. and Fishel, R. (2004) hMSH4-hMSH5 recognizes Holliday Junctions and forms a meiosis-specific sliding clamp that embraces homologous chromosomes. *Mol Cell*, **15**, 437-451.
57. Miguel, V., Monti, M.R. and Argarana, C.E. (2008) The role of MutS oligomers on Pseudomonas aeruginosa mismatch repair system activity. *DNA Repair (Amst)*, **7**, 1799-1808.
58. Curti, E., McDonald, J.P., Mead, S. and Woodgate, R. (2009) DNA polymerase switching: effects on spontaneous mutagenesis in Escherichia coli. *Mol Microbiol*, **71**, 315-331.
59. Lamers, M.H., Perrakis, A., Enzlin, J.H., Winterwerp, H.H., de Wind, N. and Sixma, T.K. (2000) The crystal structure of DNA mismatch repair protein MutS binding to a G x T mismatch. *Nature*, **407**, 711-717.
60. Obmolova, G., Ban, C., Hsieh, P. and Yang, W. (2000) Crystal structures of mismatch repair protein MutS and its complex with a substrate DNA. *Nature*, **407**, 703-710.
61. Warren, J.J., Pohlhaus, T.J., Changela, A., Iyer, R.R., Modrich, P.L. and Beese, L.S. (2007) Structure of the human MutSalpha DNA lesion recognition complex. *Mol Cell*, **26**, 579-592.
62. Groothuizen, F.S., Fish, A., Petoukhov, M.V., Reumer, A., Manelyte, L., Winterwerp, H.H., Marinus, M.G., Lebbink, J.H., Svergun, D.I., Friedhoff, P. *et al.* (2013) Using stable MutS dimers and tetramers to quantitatively analyze DNA mismatch recognition and sliding clamp formation. *Nucleic Acids Res*, **41**, 8166-8181.

63. Lamers, M.H., Georgijevic, D., Lebbink, J.H., Winterwerp, H.H., Agianian, B., de Wind, N. and Sixma, T.K. (2004) ATP increases the affinity between MutS ATPase domains. Implications for ATP hydrolysis and conformational changes. *J Biol Chem*, **279**, 43879-43885.
64. Ashkenazy, H., Abadi, S., Martz, E., Chay, O., Mayrose, I., Pupko, T. and Ben-Tal, N. (2016) ConSurf 2016: an improved methodology to estimate and visualize evolutionary conservation in macromolecules. *Nucleic Acids Res*, **44**, W344-350.
65. Blackwell, L.J., Bjornson, K.P., Allen, D.J. and Modrich, P. (2001) Distinct MutS DNA-binding modes that are differentially modulated by ATP binding and hydrolysis. *J Biol Chem*, **276**, 34339-34347.
66. Mendillo, M.L., Mazur, D.J. and Kolodner, R.D. (2005) Analysis of the interaction between the Saccharomyces cerevisiae MSH2-MSH6 and MLH1-PMS1 complexes with DNA using a reversible DNA end-blocking system. *J Biol Chem*, **280**, 22245-22257.
67. Correa, E.M., De Tullio, L., Velez, P.S., Martina, M.A., Argarana, C.E. and Barra, J.L. (2013) Analysis of DNA structure and sequence requirements for Pseudomonas aeruginosa MutL endonuclease activity. *J Biochem*, **154**, 505-511.
68. Correa, E.M., Martina, M.A., De Tullio, L., Argarana, C.E. and Barra, J.L. (2011) Some amino acids of the Pseudomonas aeruginosa MutL D(Q/M)HA(X)(2)E(X)(4)E conserved motif are essential for the in vivo function of the protein but not for the in vitro endonuclease activity. *DNA Repair (Amst)*, **10**, 1106-1113.
69. Genschel, J., Kadyrova, L.Y., Iyer, R.R., Dahal, B.K., Kadyrov, F.A. and Modrich, P. (2017) Interaction of proliferating cell nuclear antigen with PMS2 is required for MutLalpha activation and function in mismatch repair. *Proc Natl Acad Sci U S A*, **114**, 4930-4935.
70. Pillon, M.C., Babu, V.M., Randall, J.R., Cai, J., Simmons, L.A., Sutton, M.D. and Guarne, A. (2015) The sliding clamp tethers the endonuclease domain of MutL to DNA. *Nucleic Acids Res*, **43**, 10746-10759.
71. Bowers, J., Sokolsky, T., Quach, T. and Alani, E. (1999) A mutation in the MSH6 subunit of the Saccharomyces cerevisiae MSH2-MSH6 complex disrupts mismatch recognition. *J Biol Chem*, **274**, 16115-16125.
72. Junop, M.S., Obmolova, G., Rausch, K., Hsieh, P. and Yang, W. (2001) Composite active site of an ABC ATPase: MutS uses ATP to verify mismatch recognition and authorize DNA repair. *Mol Cell*, **7**, 1-12.
73. Junop, M.S., Yang, W., Funchain, P., Clendenin, W. and Miller, J.H. (2003) In vitro and in vivo studies of MutS, MutL and MutH mutants: correlation of mismatch repair and DNA recombination. *DNA Repair (Amst)*, **2**, 387-405.
74. Lebbink, J.H., Georgijevic, D., Natrajan, G., Fish, A., Winterwerp, H.H., Sixma, T.K. and de Wind, N. (2006) Dual role of MutS glutamate 38 in DNA mismatch discrimination and in the authorization of repair. *EMBO J*, **25**, 409-419.
75. Schofield, M.J., Brownewell, F.E., Nayak, S., Du, C., Kool, E.T. and Hsieh, P. (2001) The Phe-X-Glu DNA binding motif of MutS. The role of hydrogen bonding in mismatch recognition. *J Biol Chem*, **276**, 45505-45508.
76. Dufner, P., Marra, G., Raschle, M. and Jiricny, J. (2000) Mismatch recognition and DNA-dependent stimulation of the ATPase activity of hMutSalpha is abolished by a single mutation in the hMSH6 subunit. *J Biol Chem*, **275**, 36550-36555.
77. Malkov, V.A., Biswas, I., Camerini-Otero, R.D. and Hsieh, P. (1997) Photocross-linking of the NH2-terminal region of Taq MutS protein to the major groove of a heteroduplex DNA. *J Biol Chem*, **272**, 23811-23817.
78. Holmes, S.F., Scarpinato, K.D., McCulloch, S.D., Schaaper, R.M. and Kunkel, T.A. (2007) Specialized mismatch repair function of Glu339 in the Phe-X-Glu motif of yeast Msh6. *DNA Repair (Amst)*, **6**, 293-303.
79. Drotschmann, K., Yang, W., Brownewell, F.E., Kool, E.T. and Kunkel, T.A. (2001) Asymmetric recognition of DNA local distortion. Structure-based functional studies of eukaryotic Msh2-Msh6. *J Biol Chem*, **276**, 46225-46229.
80. Yamamoto, A., Schofield, M.J., Biswas, I. and Hsieh, P. (2000) Requirement for Phe36 for DNA binding and mismatch repair by Escherichia coli MutS protein. *Nucleic Acids Res*, **28**, 3564-3569.

81. Bhairosing-Kok, D., Groothuizen, F.S., Fish, A., Dharadhar, S., Winterwerp, H.H.K. and Sixma, T.K. (2019) Sharp kinking of a coiled-coil in MutS allows DNA binding and release. *Nucleic Acids Res*, **47**, 8888-8898.
82. Mendillo, M.L., Putnam, C.D., Mo, A.O., Jamison, J.W., Li, S., Woods, V.L., Jr. and Kolodner, R.D. (2010) Probing DNA- and ATP-mediated conformational changes in the MutS family of mispair recognition proteins using deuterium exchange mass spectrometry. *J Biol Chem*, **285**, 13170-13182.
83. Qiu, R., DeRocco, V.C., Harris, C., Sharma, A., Hingorani, M.M., Erie, D.A. and Weninger, K.R. (2012) Large conformational changes in MutS during DNA scanning, mismatch recognition and repair signalling. *EMBO J*, **31**, 2528-2540.
84. Sharma, A., Doucette, C., Biro, F.N. and Hingorani, M.M. (2013) Slow conformational changes in MutS and DNA direct ordered transitions between mismatch search, recognition and signaling of DNA repair. *J Mol Biol*, **425**, 4192-4205.
85. Hedglin, M. and Benkovic, S.J. (2017) Replication Protein A Prohibits Diffusion of the PCNA Sliding Clamp along Single-Stranded DNA. *Biochemistry*, **56**, 1824-1835.
86. Laurence, T.A., Kwon, Y., Johnson, A., Hollars, C.W., O'Donnell, M., Camarero, J.A. and Barsky, D. (2008) Motion of a DNA sliding clamp observed by single molecule fluorescence spectroscopy. *J Biol Chem*, **283**, 22895-22906.
87. Lenhart, J.S., Pillon, M.C., Guarne, A. and Simmons, L.A. (2013) Trapping and visualizing intermediate steps in the mismatch repair pathway in vivo. *Mol Microbiol*, **90**, 680-698.
88. Mendillo, M.L., Hargreaves, V.V., Jamison, J.W., Mo, A.O., Li, S., Putnam, C.D., Woods, V.L., Jr. and Kolodner, R.D. (2009) A conserved MutS homolog connector domain interface interacts with MutL homologs. *Proc Natl Acad Sci U S A*, **106**, 22223-22228.
89. Jacquelin, D.K., Filiberti, A., Argarana, C.E. and Barra, J.L. (2005) Pseudomonas aeruginosa MutL protein functions in Escherichia coli. *Biochem J*, **388**, 879-887.
90. Iyer, R.R., Pohlhaus, T.J., Chen, S., Hura, G.L., Dzantiev, L., Beese, L.S. and Modrich, P. (2008) The MutSalpha-proliferating cell nuclear antigen interaction in human DNA mismatch repair. *J Biol Chem*, **283**, 13310-13319.
91. Liu, L., Ortiz Castro, M.C., Rodriguez Gonzalez, J., Pillon, M.C. and Guarne, A. (2019) The endonuclease domain of Bacillus subtilis MutL is functionally asymmetric. *DNA Repair (Amst)*, **73**, 1-6.
92. Iyer, R.R., Pluciennik, A., Genschel, J., Tsai, M.S., Beese, L.S. and Modrich, P. (2010) MutLalpha and proliferating cell nuclear antigen share binding sites on MutSbeta. *J Biol Chem*, **285**, 11730-11739.

## FIGURE LEGENDS

**Figure 1. Replication DNA substrates are recognized by MutS.** (A) Representation of the DNA substrates used in the present study. Numbers indicate the nucleotides at each strand and upstream and downstream of the mismatch. SPR measurements of MutS binding to biotinylated GT-pDNA (B) and GT-dsDNA (C) immobilized on a streptavidin-derivatized sensor chip (~800 RU). Different protein concentrations are represented by different colors. The kinetics of MutS binding to GT-dsDNA was fitted using a 1:1 model, represented in black lines. Sensorgrams of MutS display solvent correction. Representative reference-subtracted curves are shown (n=3). (D-F) **Replication DNA substrates containing a mismatch alters MutS electrophoretic migration under native conditions.** MutS (2 μM) was individually incubated alone or with DNA substrates (4 μM). Reaction mixtures were analyzed on native polyacrylamide gels. (D, left panel) Representative image of a native gel showing the MutS-DNA mobility shift relative to free MutS. Migration of molecular weight markers, thyroglobulin (670 kDa), apoferritin (443 kDa) and β-amylase (200 kDa), is shown with arrows. a, b and c corresponds to the migration of MutS-GT-pDNA, free MutS, and MutS complexed with pDNA, GT-dsDNA or dsDNA bands, respectively. (D, right panel) Fraction of a, b and c bands for MutS bound to the different DNA structures. The intensity of a, b and c bands was quantified in each line to calculate the relative fraction of each band. (E) Fraction of a, b and c bands for MutS bound to GT-pDNA structures containing 8 nt to 16 nt between GT and the 3'-OH terminus of the primer strand. Control reactions without DNA (-) and GT-dsDNA (18 nt from the MM) were included. (F) Fraction of a, b and c bands for MutS bound to pDNA structures containing the twelve different MMs located 8 nt from the 3'-OH terminus of the primer strand. Control reactions without DNA (-) and pDNA (AT) were included. Data represented the means of at least triplicates. Standard deviations were <5% of the mean.

**Figure 2. MutS binding to mismatched replication DNA substrates induces a rearrangement of the protein structure.** (A-C) MutSR842E (4 μM) was individually mixed with DNA substrates (4 μM), and reaction products were analyzed on native polyacrylamide gels. (A, left panel) Representative image of a native gel showing the MutSR842E-DNA mobility shift relative to the apo MutSR842E form. Thyroglobulin (670 kDa), β-amylase (200 kDa) and bovine albumin (66 kDa) band migration is shown with arrows. a, b and c corresponds to the migration of MutSR842E-GT-pDNA, free MutSR842E, and MutSR842E complexed with pDNA, GT-dsDNA or dsDNA bands, respectively. (A, right panel) Fraction of a, b and c bands for MutSR842E bound to DNA structures. The intensity of a, b and c bands was quantified in each line to calculate the relative fraction of each band. (B) Fraction of a, b and c bands for MutSR842E bound to GT-pDNA structures containing 8 nt to 16 nt from the GT to the 3'-OH terminus of the primer strand. Control reactions without DNA (-) and GT-dsDNA (18 nt from the MM) were included. (C) Fraction of a, b and c bands for MutSR842E bound to pDNA structures containing the twelve different MMs located 8 nt from the 3'-OH terminus of the primer strand. Control reactions without DNA (-) and pDNA (AT) were included. Data represented the means of at least triplicates. Standard deviations were <5% of the mean. (D) Far-UV CD spectra of 2 μM MutS in the absence (black line) or presence of 4 μM GT-pDNA (blue line) and GT-dsDNA (grey line). The spectra plotted are the average of three independent scans. Contributions of buffer and DNA to ellipticity were subtracted. (E) Fraction of secondary structures estimated from CD spectra using the BeStSel web tool. (F) 2 μM MutS was preincubated alone or with DNA substrates (4 μM), and then subjected to partial tryptic digestion. Reactions were analyzed by SDS-PAGE, and the intensity of full-length MutS bands was quantified and used to calculate the fraction of MutS remaining. The intensity of the MutS band in the control condition without trypsin was taken as 1. Data represent mean ± standard deviation (n=3).

**Figure 3. MutS contains a novel putative DNA interaction site for DNA replication structures.** (A) Cartoon representation of the *E. coli* MutSD835R crystal structure (PDB entry: 3ZLJ). One monomer is shown in gray and the other is coloured by domain. Mismatch binding domain (8), connector domain (green), core domain (light-blue), clamp domain (dark-blue), ATPase domain (orange) and HTH domain (purple). The C-terminal domain is not shown for simplicity. (B) Putative DNA binding sites according to BindUp. Ribbon diagram of *E. coli*

MutSD835R (blue) showing predicted DNA binding residues (surface representation, red). One of the sites was in the upper channel of MutS (light-red, referred here as DNA binding site I). Other of the putative binding sites was located in the ATPase and HTH domains (light-red). The lower channel shows the putative binding site referred here on as DNA binding site II (dark-red). Front (C) and lateral (D) view of the 3D structure of *E. coli* MutSΔ800 with docked GT-dsDNA. (E) Close view of DNA binding site I in the *E. coli* MutSΔ800 bound GT-dsDNA structure, showing the GT mismatch (blue) and the Phe 36 and Glu 38 residues (yellow). Front (F) and side (G) view of the 3D docked structure of GT-pDNA to *E. coli* MutSΔ800. (H) Residues (light-yellow) from the DNA binding site II contacted the double-stranded and single-stranded regions of the GT-pDNA, while the Arg 275 residue (dark-yellow) interacted with the 3'-OH terminus of the primer strand. (I) Close view of the interaction between the 3'-OH terminus of GT-pDNA and the Arg 275 residue (cyan, blue and red) in the DNA binding site II. *E. coli* MutSΔ800 is represented by ribbons diagrams (grey). DNAs are showed in a space-filling model. DNA backbone is shown in red, and the GT mismatch is highlighted in blue.

**Figure 4. Mutation of Arg 272 in MutS alters DNA-binding and ATPase activities, and is associated with a defective antimutagenic activity *in vivo*.** (A-D) SPR measurements of MutSR272E and MutSF33A binding to DNA structures. MutS mutants (0.16-2.50 µM) were individually flowed over surface-immobilized GT-pDNA (A and C) or GT-dsDNA (B and D) (~1100 RU). Different protein concentrations are represented by different colors. Sensorgrams of MutS mutants display solvent correction. Representative reference-subtracted curves are shown (n=3). (E) ATP hydrolysis by wild-type and MutS mutants was measured by quantifying the free phosphate released in parallel reactions containing MutS proteins (0.02-1.28 µM) and ATP (400 µM). (F) Mutation rates to resistance to ciprofloxacin ($Cip^r$, $10^{-8}$), rifampicin ($Rif^r$, $10^{-8}$) and amikacin ($Amk^r$, $10^{-6}$) and 95% confidence limits were estimated for PAO1 *mutS* carrying empty pEx, pEX-*mutS*, pEX-*mutS*R272E or pEX-*mutS*F33A. Error bars represent the upper and lower 95% confidence intervals. No overlap of 95% confidence intervals indicates statistically significant differences.

**Figure 5. MutS remains associated with replication DNA structures containing a mismatch in the presence of ATP.** MutS was injected over a chip surface with GT-pDNA (A) or GT-dsDNA (B) for 80-100 s. After MutS binding, buffer alone and buffer containing 5 mM ATP were successively flowed over sensors for 180 s and 85 s, respectively. MutS concentrations were 0.6 and 1.2 µM in A and 1.2 and 2.5 µM in B. Sensograms of MutS display solvent correction. Representative reference-subtracted curves are shown (n=3). (C, D) ATP hydrolysis by MutS (40 nM) was measured in the absence or presence of DNA (1.6 µM) as a function of ATP concentration (3-400 µM). Data represent mean ± standard deviation (n=3).

**Figure 6. MutS interaction with MutL is modulated by the replication GT-pDNA structure.** (A) Spots of $His_6$-tagged MutL and β clamp (3, 6 and 12 pmol) on nitrocellulose membranes were incubated with soluble *Strep* II-tagged MutS (0.5 µM). (B) *Strep* II-tagged MutS (3, 6 and 12 pmol) alone or preincubated with GT-pDNA or GT-dsDNA was spotted on nitrocellulose and then, incubated with soluble $His_6$-tagged MutL (0.25 µM). Binding of soluble proteins was detected using a mouse anti-*Strep* II or $His_6$ monoclonal antibody. The fluorescence intensity of the spots was quantified using the Gel-Pro analyzer software. **MutL endonuclease activity is stimulated by MutS but not by β clamp.** (C) GT-pDNA or GT-dsDNA (1 µM) were incubated with increasing concentrations of MutL (0.13-1.3 µM) for 2 h. Negatives of representative ethidium bromide-stained photographs are shown (upper panel). The first well is a control of DNA incubated without MutL (-). A control reaction containing the highest MutL concentration (1.3 µM) and EDTA was carried out (EDTA). Bands were quantified and the amount of remaining DNA was plotted against MutL concentration. (D) MutL (0.13 µM) was incubated with DNA (1 µM) in the absence or presence of equimolar MutS or β clamp. Negatives of representative ethidium bromide-stained photographs are shown (upper panel). Bands were quantified and the amount of remaining DNA was plotted for each condition. Data represent mean ± standard deviation (n=3).

**Figure 7. Proposed model for regulation of specialized DNA polymerases and mismatch repair pathway choice.** Our model illustrates how the action of the MutS dimer in RSP and MMR pathways depends on DNA structures (mismatched pDNAs vs dsDNAs), interacting protein partners (β clamp vs MutL) and nucleotide bound (ADP vs ATP). See Discussion text for details regarding this model.

# Figure 1

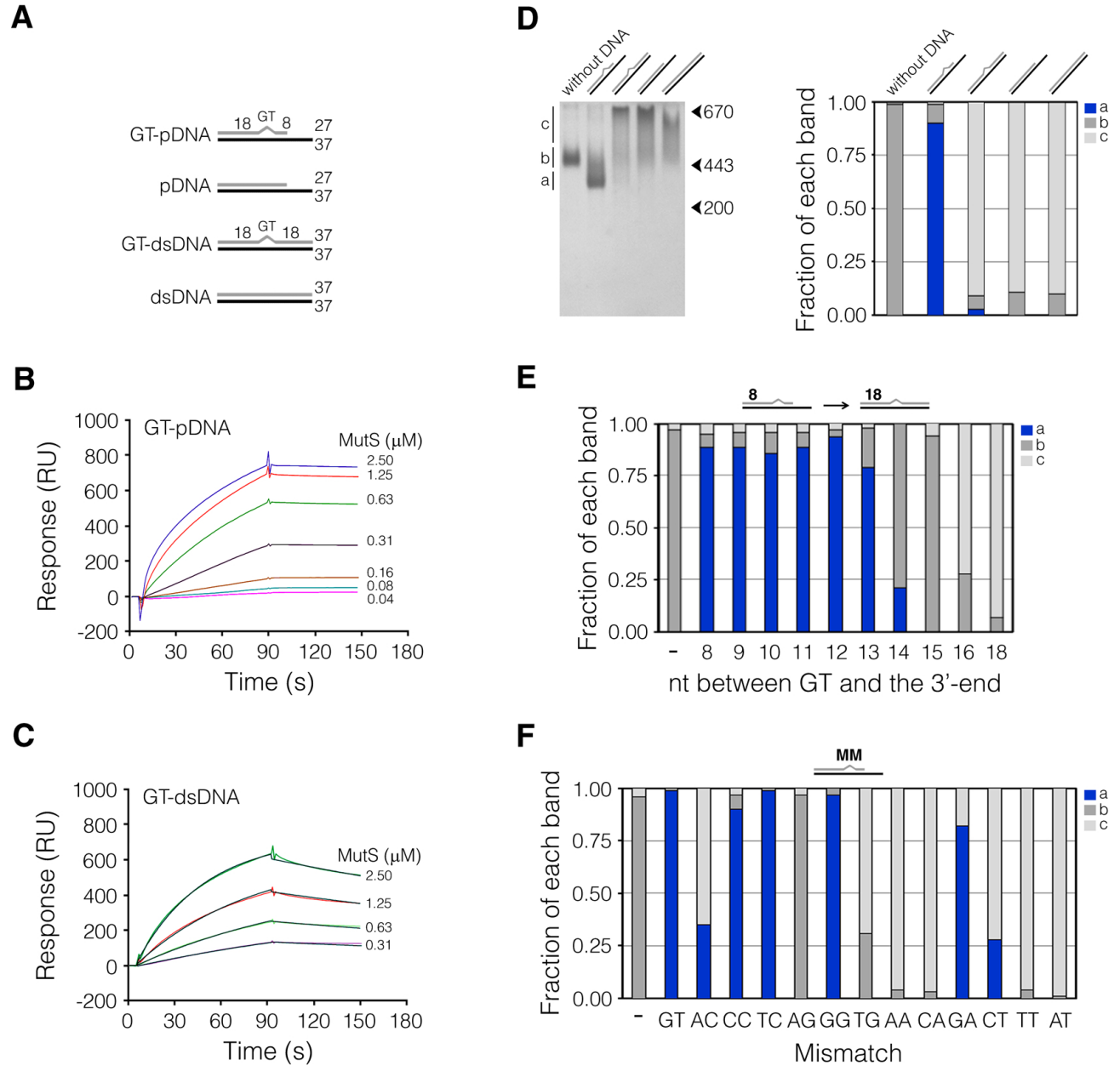
A
GT-pDNA
18 GT 8
27
37
pDNA
27
37
GT-dsDNA
18 GT 18
37
37
dsDNA
37
37
B
GT-pDNA
MutS (μM)
2.50
1.25
0.63
0.31
0.16
0.08
0.04
Response (RU)
Time (s)
C
GT-dsDNA
MutS (μM)
2.50
1.25
0.63
0.31
Response (RU)
Time (s)
D
without DNA
c
b
a
670
443
200
Fraction of each band
a
b
c
E
8
18
Fraction of each band
nt between GT and the 3'-end
F
MM
Fraction of each band
Mismatch
GT AC CC TC AG GG TG AA CA GA CT TT AT

# Figure 2

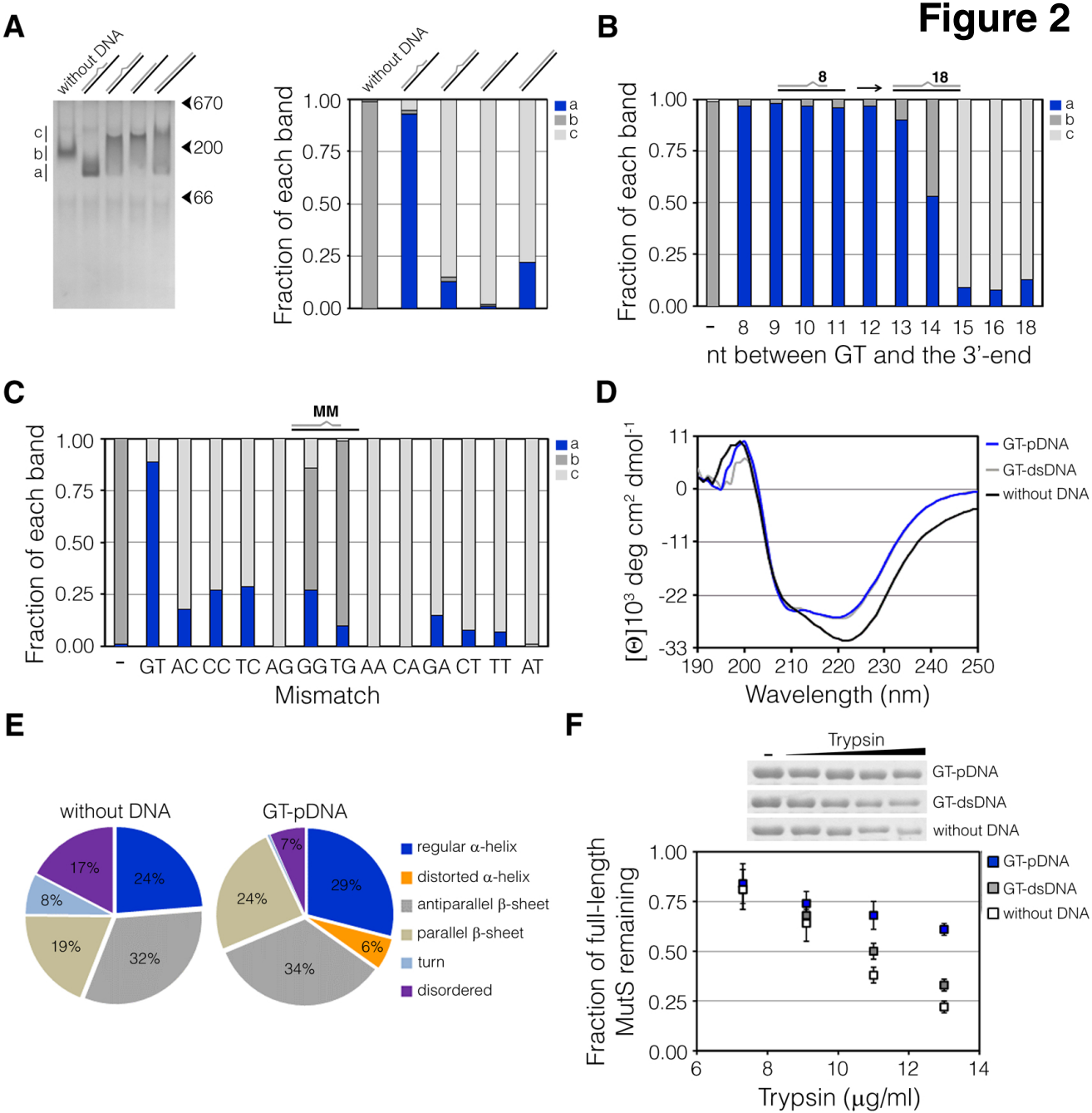
A
without DNA
670
200
66
c
b
a
Fraction of each band
1.00
0.75
0.50
0.25
0.00
a
b
c
B
8
18
- 8 9 10 11 12 13 14 15 16 18
nt between GT and the 3'-end
C
MM
- GT AC CC TC AG GG TG AA CA GA CT TT AT
Mismatch
D
GT-pDNA
GT-dsDNA
without DNA
[Θ]10³ deg cm² dmol⁻¹
11
0
-11
-22
-33
190 200 210 220 230 240 250
Wavelength (nm)
E
without DNA
GT-pDNA
24%
32%
19%
8%
17%
29%
6%
34%
24%
7%
regular α-helix
distorted α-helix
antiparallel β-sheet
parallel β-sheet
turn
disordered
F
Trypsin
-
GT-pDNA
GT-dsDNA
without DNA
Fraction of full-length MutS remaining
6 8 10 12 14
Trypsin (μg/ml)

Figure 3

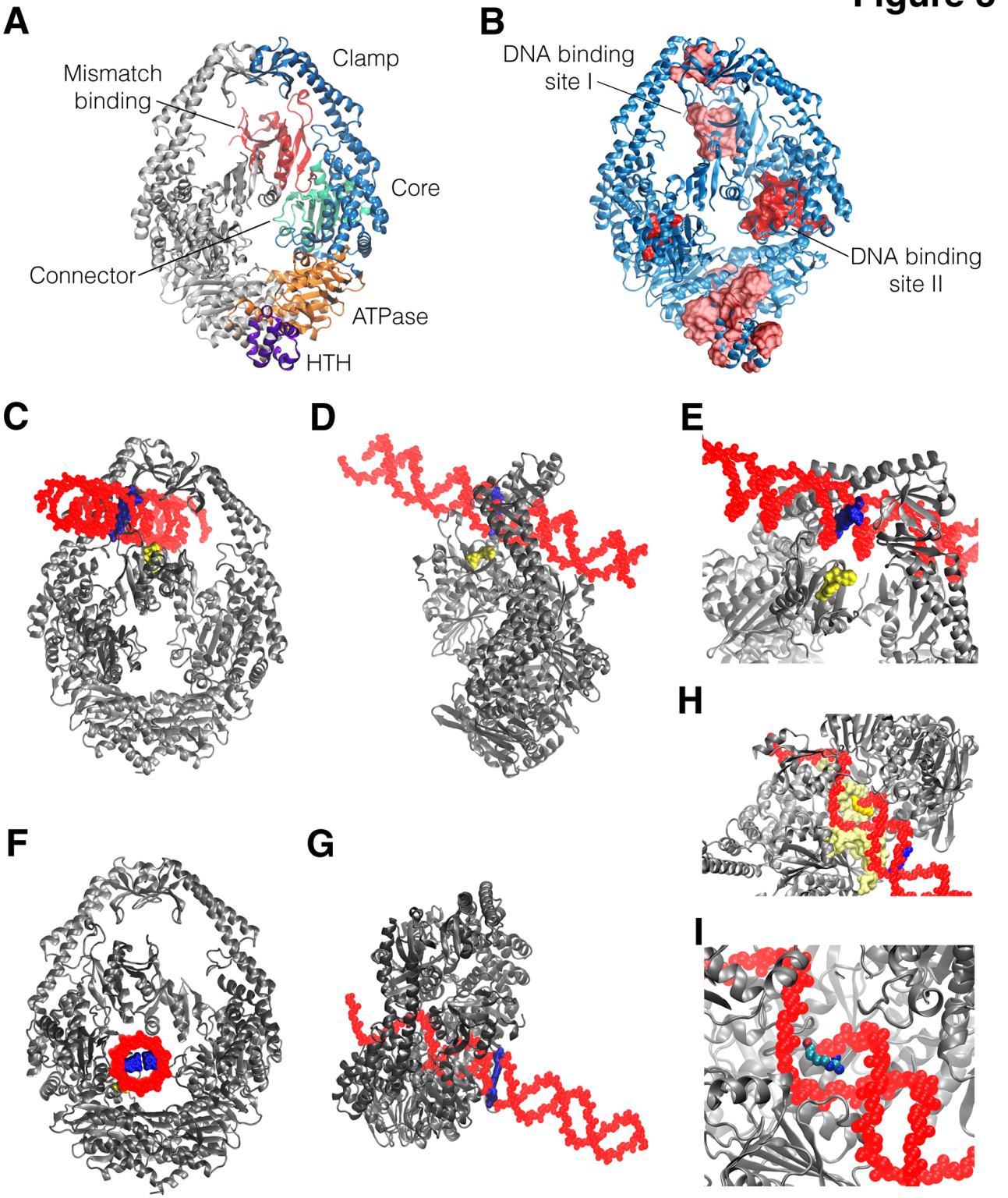
A
Mismatch binding
Clamp
Core
Connector
ATPase
HTH
B
DNA binding site I
DNA binding site II
C
D
E
H
F
G
I

# Figure 4

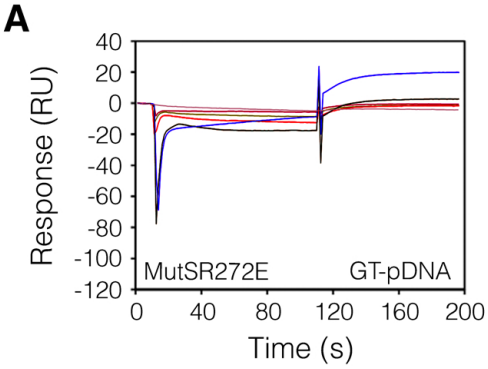
A
Response (RU)
40
20
0
-20
-40
-60
-80
-100
-120
MutSR272E
GT-pDNA
0
40
80
120
160
200
Time (s)

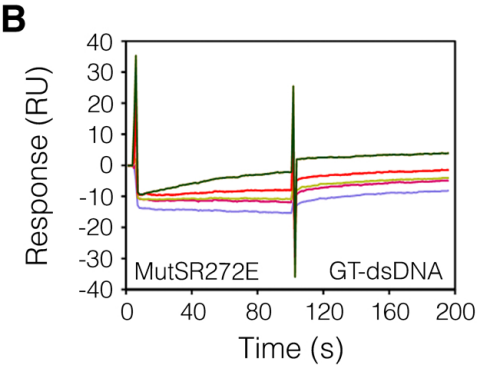
B
Response (RU)
40
30
20
10
0
-10
-20
-30
-40
MutSR272E
GT-dsDNA
0
40
80
120
160
200
Time (s)

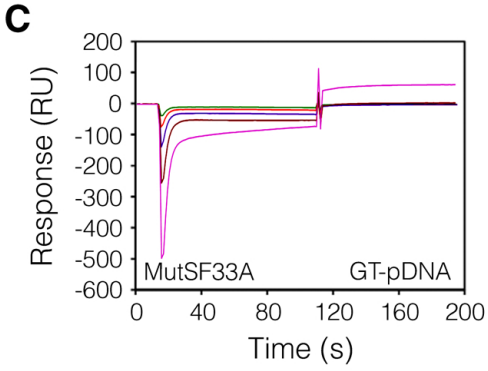
C
Response (RU)
200
100
0
-100
-200
-300
-400
-500
-600
MutSF33A
GT-pDNA
0
40
80
120
160
200
Time (s)

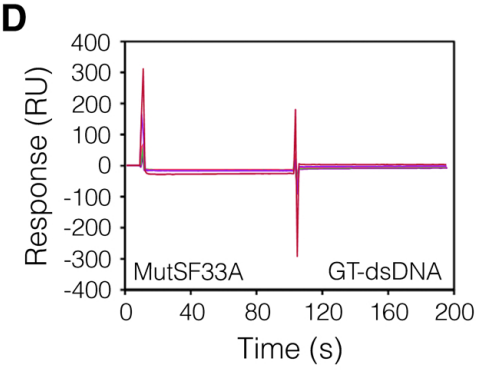
D
Response (RU)
400
300
200
100
0
-100
-200
-300
-400
MutSF33A
GT-dsDNA
0
40
80
120
160
200
Time (s)

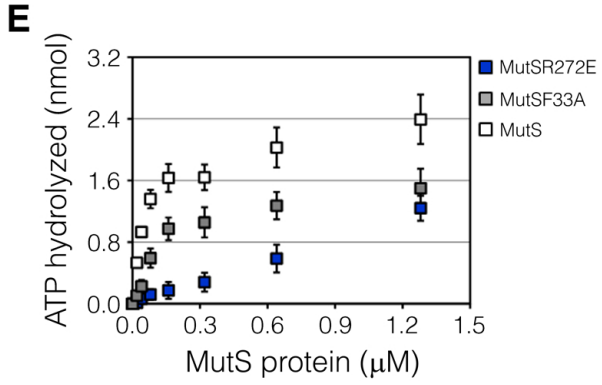
E
ATP hydrolyzed (nmol)
3.2
2.4
1.6
0.8
0.0
0.0
0.3
0.6
0.9
1.2
1.5
MutS protein (μM)
MutSR272E
MutSF33A
MutS

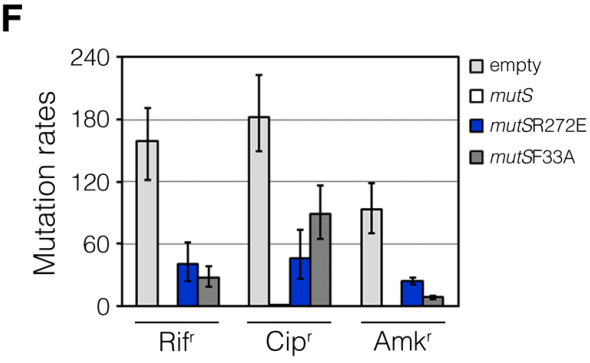
F
Mutation rates
240
180
120
60
0
Rifr
Cipr
Amkr
empty
mutS
mutSR272E
mutSF33A

# Figure 5

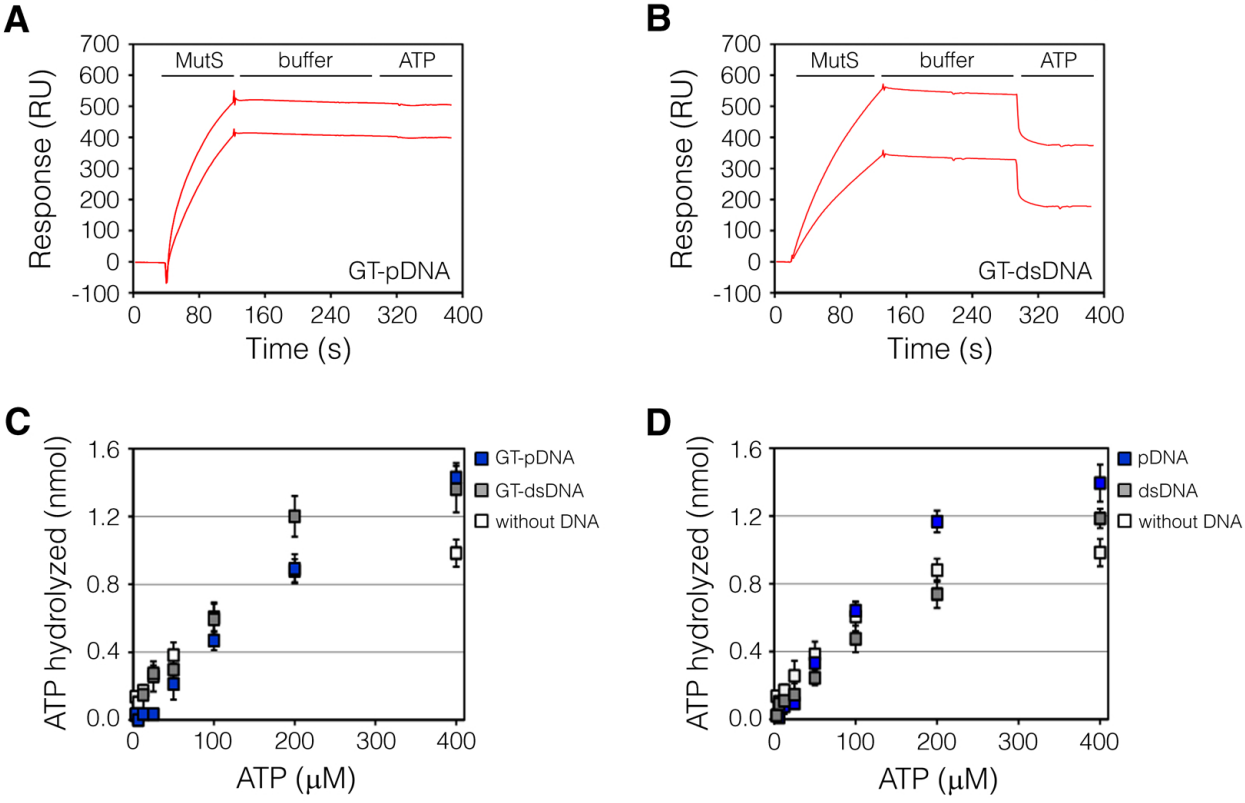
A
MutS
buffer
ATP
Response (RU)
Time (s)
GT-pDNA
B
MutS
buffer
ATP
Response (RU)
Time (s)
GT-dsDNA
C
ATP hydrolyzed (nmol)
ATP (μM)
GT-pDNA
GT-dsDNA
without DNA
D
ATP hydrolyzed (nmol)
ATP (μM)
pDNA
dsDNA
without DNA

# Figure 6

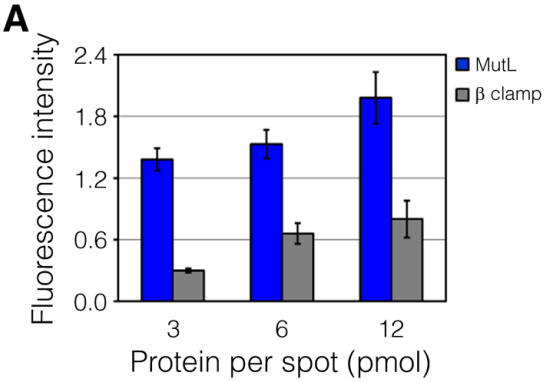
A
Fluorescence intensity
2.4
1.8
1.2
0.6
0.0
3
6
12
Protein per spot (pmol)
MutL
β clamp

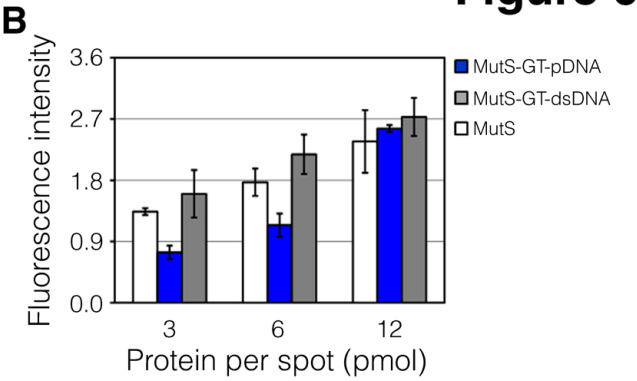
B
Fluorescence intensity
3.6
2.7
1.8
0.9
0.0
3
6
12
Protein per spot (pmol)
MutS-GT-pDNA
MutS-GT-dsDNA
MutS

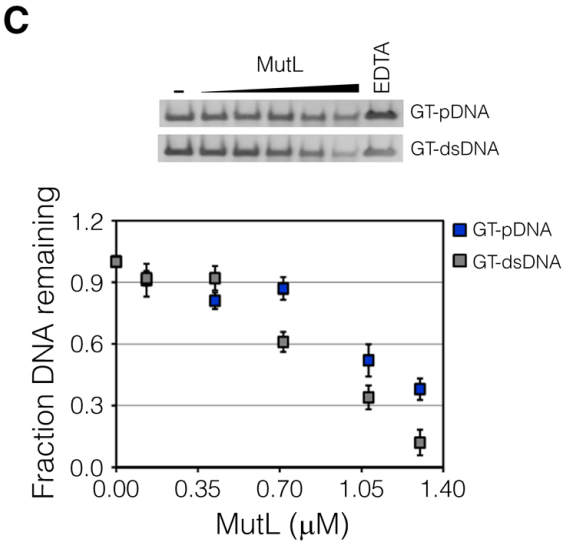
C
MutL
EDTA
–
GT-pDNA
GT-dsDNA
Fraction DNA remaining
1.2
0.9
0.6
0.3
0.0
0.00
0.35
0.70
1.05
1.40
MutL (μM)
GT-pDNA
GT-dsDNA

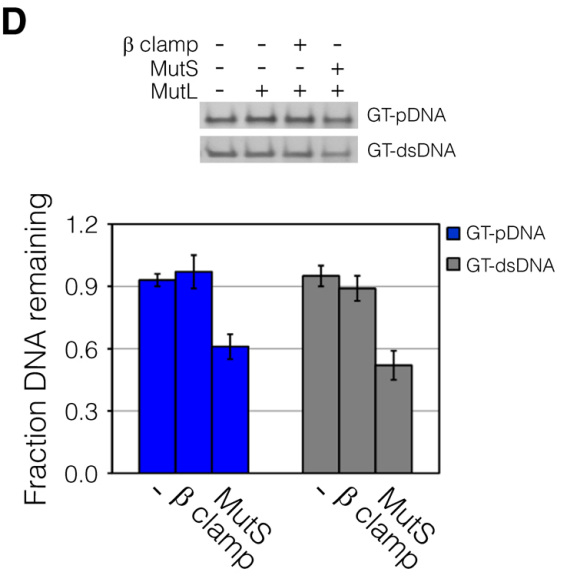
D
β clamp - - + -
MutS - - - +
MutL - + + +
GT-pDNA
GT-dsDNA
Fraction DNA remaining
1.2
0.9
0.6
0.3
0.0
- β clamp
MutS
- β clamp
MutS
GT-pDNA
GT-dsDNA

# Figure 7

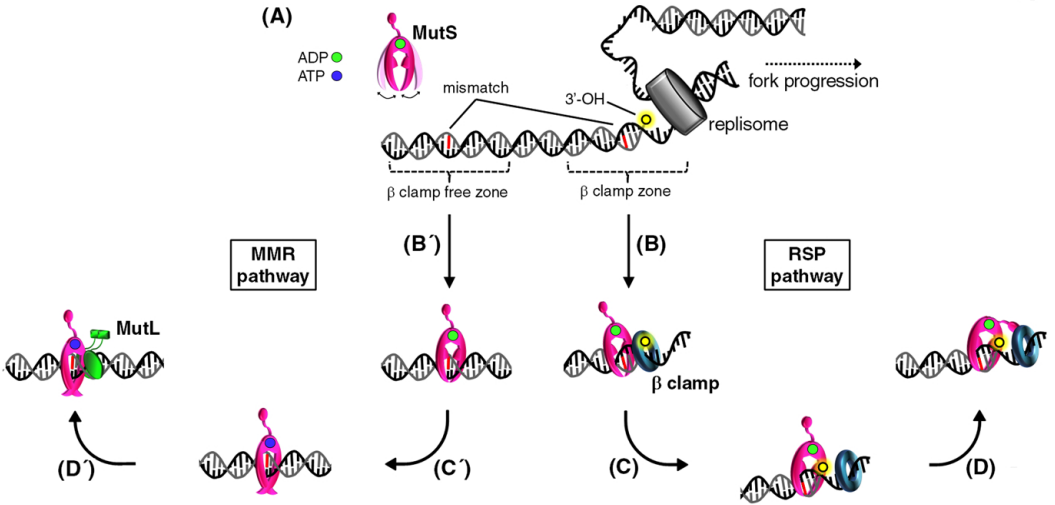
(A)
MutS
ADP
ATP
mismatch
3'-OH
fork progression
replisome
β clamp free zone
β clamp zone
MMR pathway
(B´)
(B)
RSP pathway
MutL
β clamp
(D´)
(C´)
(C)
(D)